Within- and between-subject reproducibility and variability in multi-modal, longitudinal brain networks

Johan Nakuci[a]*, Nick Wasylyshyn[b,c], Matthew Cieslak[d], James C. Elliot[d], Kanika Bansal[b,e], Barry Giesbrecht[d,f], Scott T. Grafton[d,f], Jean M. Vettel[b,c,d], Javier O. Garcia[b,c], Sarah F. Muldoon[a,g]*

[a] Neuroscience Program, University at Buffalo, SUNY, Buffalo, NY 14260, USA
[b] U.S. CCDC Army Research Laboratory, Aberdeen Proving Ground, MD 21005, USA
[c] Department of Bioengineering, University of Pennsylvania, Philadelphia, PA 19104, USA
[d] Department of Psychological and Brain Sciences, University of California, Santa Barbara, CA 93106, USA
[e] Department of Biomedical Engineering, Columbia University, New York, NY 10027, USA
[f] Institute for Collaborative Biotechnologies, University of California, Santa Barbara, CA 93106, USA
[g] Department of Mathematics and CDSE Program, University at Buffalo, SUNY, Buffalo, NY 14260 USA

*Corresponding Authors:
Johan Nakuci
Department of Mathematics
244 Mathematics Building
UB North Campus
Buffalo NY, 14260-2900
Tel: 716-645-6284
Fax: 1-716-645-5039
jnakuci@buffalo.edu

Sarah F. Muldoon, PhD
Department of Mathematics
Neuroscience and CDSE Programs
244 Mathematics Building
UB North Campus
Buffalo NY, 14260-2900
Tel: 1-716-645-8774
Fax: 1-716-645-5039
smuldoon@buffalo.edu

43   **Abstract**

44   Network analysis provides new and important insights into the function of complex

45   systems such as the brain by examining structural and functional networks constructed from

46   diffusion Magnetic Resonance Imaging (dMRI), functional MRI (fMRI) and

47   Electro/Magnetoencephalography (E/MEG) data. Although network models can shed light on

48   cognition and pathology, questions remain regarding the importance of these findings, due in

49   part to the reproducibility of the core measurements and subsequent modeling strategies. In order

50   to ensure that results are reproducible, we need a better understanding of within- and between-

51   subject variability over long periods of time. Here, we analyze a longitudinal, 8 session, multi-

52   modal (dMRI, and simultaneous EEG-fMRI), and multiple task imaging data set. We first

53   investigate the reproducibility of individual brain connections and network measures and find

54   that across all modalities, within-subject reproducibility is higher than between-subject

55   reproducibility, reaffirming the ability to detect individual differences in network structure in

56   both structural and functional human brain networks. We see high variability in the

57   reproducibility of pairwise connections between brain regions, but observe that in EEG-derived

58   networks, during both rest and task, alpha-band connectivity is consistently more reproducible

59   than networks derived from other frequency bands. Further, reproducible connections correspond

60   to strong connections. Structural networks show a higher reliability in network statistics than

61   functional networks, and certain measures such as synchronizability and eigenvector centrality

62   are consistently less reliable than other network measures across all modalities. Finally, we find

63   that structural dMRI networks outperform functional networks in their ability to identify

64   individuals using a fingerprinting analysis. Our results highlight that functional networks likely

65   reflect state-dependent variability not present in structural networks, and that the analysis of

2

66   either structural or functional networks to study individual differences should depend on whether

67   or not one wants to take into account state dependencies of the observed networks.

68

71 **1 Introduction**

72   The introduction of network theory to neuroscience has increased our understanding of

73 the brain's functional and structural organization. This powerful tool has given new insights into

74 how higher order brain functions arise (Bassett and Sporns, 2017; Park and Friston, 2013) and

75 how changes can lead to pathology (Fornito et al., 2015). However, questions have been raised

76 regarding the reliability of brain network properties given the effects of noise in the signal,

77 particularly in fMRI (Laumann et al., 2016; Power et al., 2018, 2012). Still, despite the presence

78 of noise, brain networks have been found to exhibit consistent properties over time among

79 individual network connections and in higher order properties, such as the clustering coefficient,

80 characteristic path length, and assortativity, for structural connectivity as measured with dMRI

81 (Bassett et al., 2011; Bonilha et al., 2015; Buchanan et al., 2014; Bürgel et al., 2006; Malykhin et

82 al., 2008), fMRI (Amunts et al., 2000; Braun et al., 2012; Deuker et al., 2009; Du et al., 2015;

83 Elliott et al., 2019; Gordon et al., 2017; Gratton et al., 2018; Laumann et al., 2015; Mangin et al.,

84 2004; Noble et al., 2017, 2019; Pannunzi et al., 2017; Rypma and D'Esposito, 1999; Shah et al.,

85 2016) and EEG/MEG (Deuker et al., 2009; Hardmeier et al., 2014; Kuntzelman and Miskovic,

86 2017). Unfortunately, most studies thus far have been limited to the analysis of a single imaging

87 modality and/or few scanning sessions, raising questions about how reliable these properties are

88 over longer times and across modalities.

89   While it is clear that there is some level of reliability in network properties within an

90 individual over time, it is also important to understand how the state of the brain (e.g., resting

91 wakefulness versus active task situations (Fox et al., 2005)), and the neural methodology (e.g.,

92 fMRI versus EEG) contributes to this reliability across multiple days. The "resting" brain (e.g.,

93 default mode network) is a state that has been shown to be metabolically demanding (Raichle et

94 al., 2001) and associated not only with task performance (e.g., Tian et al., 2012) but also disease

95 (e.g., Sorg et al., 2007), very much similar to task-related activity; however, the "resting" brain is

96 fundamentally different from task-related activity, as engagement in a task requires precise

97 recruitment of and coordination between regions of the brain (Fox et al., 2005). Also, in a field

98 with a variety of diverse methodologies (e.g., fMRI, EEG, MEG, PET, etc), neuroscience

99 researchers draw conclusions from methods that are measuring fundamentally different neural

100 properties. For example, fMRI is an indirect measurement of neural activity, as it measures

101 oxygenation and neural activity is inferred. Whereas EEG, a "direct" measurement, is measured

102 on the scalp and filtered by a variety of tissues and bone separating the scalp from the brain. In

103 terms of reliability, experimental design and task demands have shown to contribute to reliability

104 in fMRI (Bennett and Miller, 2013, 2010), and EEG suffers from a large variety of factors that

105 could impact reliability as well (McEvoy et al., 2000). However, there is no study, to our

106 knowledge, that has measured reliability of network structure derived from both fMRI and EEG

107 data collected at the same time over many sessions.

108   In addition to studying reliability within an individual over time, one can also ask about

109 how network properties differ between individuals. Indeed, recent work has shown that brain

110 networks can provide insight into the unique features associated with a person (Bansal et al.,

111 2018b, 2018a; Gordon et al., 2017; Seitzman et al., 2019). A giant leap toward the goal of

112 understanding differences in brain networks was made with the finding that functional brain

113 activity has unique features that can identify a person in a group, similar to a fingerprint (Finn et

114 al., 2015). This fingerprinting property has also been found in structural connectomes (Powell et

115 al., 2018; Yeh et al., 2016). Fingerprinting is important because it allows neuroimaging analyses

116 to focus on the individual and not only on group-level differences (Finn et al., 2015).

117 To further understand reliability in brain networks over time, across different states, and

118 across modalities, we quantified within- and between-subject reliability in a rich longitudinal and

119 multi-modal dataset consisting of dMRI and simultaneous EEG-fMRI recording during resting-

120 state and multiple tasks. Importantly, the data set studied here was part of a larger study

121 examining naturalistic sleep variability in individuals (Thurman et al., 2018). Here, we do not

122 focus on the effects of variation in sleep pressure, but instead note that due to the study design,

123 subjects varied in the amount of sleep pressure they experienced during each imaging session,

124 presumably augmenting variability within- and between-subjects' functional brain network over

125 time. We examine both structural and functional brain networks in this data set to study

126 reliability of individual connections and higher order network statistics. To create structural

127 networks, dMRI imaging was used to perform tractography and network connections were

128 defined as the density of streamlines between brain regions. fMRI networks were constructed

129 using the Pearson-Product Correlation to quantify the magnitude of the statistical relationship in

130 the BOLD signal between brain regions. For EEG, the time-series signal from each sensor was

131 first separated into traditional frequency bands of δ (1-3 Hz), θ (4-7 Hz), α (8-13 Hz), β (14-30

132 Hz) and γ (30-60 Hz), and functional connectivity was calculated using the debiased-weighted

133 Phase-Lag Index (dwPLI) which quantifies phase synchronization between sensors based on the

134 consistency of the lag between the instantaneous phases of two sensors (Vinck et al., 2011).

135 In the current work we evaluate: 1) which brain connections and network measures are

136 most reliable within- and between-individuals; 2) how reliability varies across state and

137 modality; and 3) how the different imaging modalities, dMRI, fMRI, and EEG, perform in a

138 fingerprinting analysis to identify an individual.

139

2 Material and methods

2.1 Participants

The University of California, Santa Barbara (UCSB) Human Subjects Committee (#16–0154) and Army Research Laboratory Human Research Protections Office (#14–098) approved all procedures, and all participants provided informed written consent. Research was conducted in accordance with the declarations of Helsinki. The data presented in this manuscript represent a subset of data collected as part of a large-scale, longitudinal experimental that collected bi-weekly structural and functional brain data. A full description of the study can be found in (Thurman et al., 2018). Here we analyze data from 27 healthy participants who were recruited by word of mouth and local advertisements. Note that by study design, participants were excluded from the multi-session segment of the study if they did not experience sleep variability. Data is accessible upon request as far as allowed by the security policy and guidelines established with the ethics committee of the US Army Research Laboratory Human Research Protection Program.

2.2 Data Description

Over the course of 16 weeks, subjects were asked to complete 8 recording sessions involving dMRI and simultaneous EEG-fMRI. For each session, simultaneous EEG-fMRI recording consisted of a 5-minute resting state and 10 tasks with varying levels of cognitive demand; specifically:

Dot Probe Task (Dot) (Sipos et al., 2014);

Dynamic Attention Task (DYN 1-4) with four repetitions of the same task (Yantis et al., 2002);

Modular Math (MOD) (Mattarella-Micke et al., 2011);

7

163   Psychomotor Vigilance Task (PVT) (Loh et al., 2004), and;

164   Visual Working Memory (VWM 1-3) with three repetitions of the same task (Luck and Vogel,

165   1997).

166   Table 1 shows the average number of subjects and sessions for each imaging modality.

167   When analyzing the EEG-fMRI data, we analyzed only six sessions of data. This was done in

168   order to make a trade-off between maximizing the number of subjects and number of sessions,

169   since not all subjects participated in all 8 sessions. Detailed information on the number of

170   subjects and sessions for functional data can be found in Tables 2 and 3. Lastly, for the

171   fingerprinting analysis using dMRI data, we used 25 subjects, all of which had an equal number

172   of sessions (8 sessions). For the fingerprinting analysis using fMRI data, 15 subjects were

173   included with all 6 sessions of resting-state and task recordings, and for the EEG data, we used

174   26 subjects with resting-state and all tasks over 6 sessions.

Table 1. Average number of subjects and sessions per imaging modality

Imaging Modality	Subjects	Sessions
dMRI	25	8
fMRI	23.1	6
EEG	27	6

Table 2. Number of subjects and sessions for each task per EEG and fMRI

Task	EEG Subjects	fMRI Subjects	Sessions
Resting-State	27	26	6
DOT	27	25	6
DYN-1	27	27	6
DYN-2	27	27	6
DYN-3	27	26	6
DYN-4	27	20	6
MOD	27	17	6
PVT	27	19	6
VWM-1	27	27	6
VWM-2	27	23	6
VWM-3	27	17	6

Table 3. Number of subjects and sessions for fingerprinting

Fingerprinting	Subjects	Sessions	Tasks Included
dMRI	25	8	n/a
fMRI	15	6	Yes
EEG	27	6	Yes

175

176 *2.3 fMRI Acquisition and Preprocessing*

177   Functional neuroimaging data were acquired on a 3T Siemens Prisma MRI using an

178 echo-planar imaging (EPI) sequence (3mm slice thickness, 64 coronal slices, field of view

179 (FoV)=192 x 192 mm, repetition time (TR)=910 ms, echo time (TE)=32 ms, flip angle=52º, and

180 voxel size: 3 x 3 x 3 mm). For repeated scans, a T1-weighted structural image was also acquired

181 using a high-resolution magnetization prepared rapid acquisition gradient echo (MPRAGE)

182 sequence (TR= 2500 ms, TE=2.22 ms, and FoV= 241 x 241 mm with a spatial resolution of .9 x

183 .9 x .9 mm), for use in coregistration and normalization.

184   fMRI BOLD images were preprocessed using Advanced Normalization Tools (ANTs)

185 (Avants et al., 2009). Physiological artifacts including respiration and cardiac cycle effects were

186 corrected using the retrospective correction of physiological motion effects method,

187 RETROICOR (Glover et al., 2000), implemented in MEAP v1.5 (Cieslak et al., 2018). Head

188 motion was estimated using antsMotionCorr, and the motion correction was completed as

189 follows: (1) An unbiased BOLD template was created within each session by averaging the

190 motion-corrected BOLD time series from each run. (2) The BOLD templates were coregistered

191 to the corresponding T1-weighted high resolution structural images, collected in each session. (3)

192 Each session was spatially normalized to a custom study-specific multi-modal template which

193 included T1-weighted, T2-weighted and GFA images from twenty-four quasi-randomly selected

194 participants chosen to match the study population. (4) The template was then affine-transformed

9

195   to the coordinate space of the MNI152 Asymmetric template. (5) Finally, the fMRI volumes

196   were transformed using the estimated head motion correction, BOLD template coregistration,

197   BOLD-to-T1w coregistration and spatial normalization into MNI space using a single Hamming

198   weighted sinc interpolation. After these transformations, the final step in the preprocessing was

199   to extract time-series from fMRI scans for functional connectivity analyses. Two atlases were

200   used to reduce the 3D volume data into 221 nodal time series data: (1) the cortical Schaefer 200

201   atlas (Schaefer et al., 2018) which was derived from intrinsic functional connectivity in resting

202   state fMRI and (2) 21 subcortical regions from the Harvard-Oxford atlas based on anatomical

203   boundaries (Makris et al., 2006). As the atlases are in MNI coordinate space, voxels within each

204   labelled region of the atlases were simply averaged, and time series were extracted for the

205   following connectivity analyses.

206   To assess functional connectivity among ROIs, mean regional time-courses were

207   extracted and standardized using the nilearn package (Abraham et al., 2014) in Python 2.7, and

208   confound regression was then conducted. In particular, the time series for each region was

209   detrended by regressing the time series on the mean as well as both linear and quadratic trends.

210   There were a total of 16 confound regressors, which included: head motion, global signal, white

211   matter, cerebrospinal fluid and derivatives, quadratics and squared derivatives. This functional

212   connectivity preprocessing pipeline was selected based on conclusions from prior work that

213   examined performance across multiple commonly used preprocessing pipelines for mitigating

214   motion artifact in functional BOLD connectivity analyses (Ciric et al., 2017; Lydon-Staley et al.,

215   2018).

216   To construct the fMRI networks, the signal from all voxels within a brain region were

217   averaged, and the Pearson Product Correlation (R) between two brain regions was calculated as

10

218
$$R = \frac{cov(x,y)}{\sqrt{\sigma_x \sigma_y}}, \qquad (1)$$

219 where x and y represent the time-series data from two different regions and σ is the variance of

220 the time series. To account for negative correlations, the absolute value of the correlations was

221 used to construct weighted functional connectivity matrices.

222

223 *2.4 EEG Acquisition and Preprocessing*

224 Continuous EEG recordings were captured simultaneously with an fMRI-compatible

225 EEG equipped with standard Ag/AgCI electrodes from 64 sites on the scalp oriented in a 10-20

226 scheme system (Brain Products, Gilching, Germany). Initial fMRI pulse and

227 ballistocardiographic artifact correction was completed in BrainAnalyzer 2 (Brain Products,

228 Gilching, Germany) using classic subtraction and filtering approaches (Allen et al., 2000, 1998).

229 These mid-level processed EEG measurements were then further processed using in-house

230 software in MATLAB (Mathworks, Inc., Natick, MA, USA) and the EEGLAB toolbox (Delorme

231 and Makeig, 2004; Mullen et al., 2013). Despite the subtraction and filtering approaches applied,

232 residual artifact from the fMRI pulse persisted. To remove these lingering artifacts, we

233 developed a new cleaning pipeline.

234 Our cleaning pipeline included steps tailored to remove common EEG artifact (e.g., eye

235 blinks, muscle-related activity) and then targeted the high frequency noise in the 16-19 Hz and

236 34-38 Hz range. EEG data were bandpass filtered between 0.75 Hz and 50 Hz using a Finite

237 Impulse Response (FIR) filter. Next, EEGLAB's automated clean_rawdata function was used to

238 determine channels that differed substantially from the estimated signal (derived from other

239 channels) or had consistent flat-lining. Then, the EEG data were subjected to an Independent

240   Component Analysis (ICA) decomposition and the ADJUST algorithm (Mognon et al., 2011)

241   was used to remove ICA components associated with stereotyped noise. Following ICA

242   decomposition, bad channels were interpolated using spherical interpolation. As a final step in

243   EEG preprocessing, the EEG data were subjected to Artifact Subspace Reconstruction (ASR)

244   (Chang et al., 2020; Mullen et al., 2015), which we used to target the aforementioned residual

245   high frequency noise from the fMRI artifact. This method, in combination with the ICA cleaning

246   method allows for the targeting of both stationary and non-stationary persistent artifacts. To

247   deploy ASR on the dataset, we first created a "clean" reference signal from each subject's EEG

248   data by: 1) concatenating EEG segments that were at least 1000ms long with amplitude below

249   100μV, (2) and notch filtering (FIR) the EEG between 16-19 Hz and 34-38 Hz. Following the

250   creation of the reference signal, ASR was then used to reconstruct the EEG that contained large

251   fluctuations greater than 5 standard deviations beyond the reference signal (in 500ms chunks).

252   Lastly, the data were re-referenced to a common average reference.

253   To construct EEG networks, the signal from each sensor was separated into standard

254   frequency bands corresponding to δ (1-3Hz), θ (4-7Hz), α (8-13Hz), β (15-30Hz) and γ (30-

255   60Hz) with a Butterworth filter (8th order) followed by Hilbert transformation. Weighted

256   functional connectivity adjacency matrices were constructed for each frequency band using the

257   de-biased weighted phase-lag index (dwPLI) (Vinck et al., 2011). Each node in the adjacency

258   matrix corresponds to a channel with the weight representing the strength (phase-lag) of the

259   connection. Specifically, dwPLI is calculated as,

260
$$dwPLI = \frac{\sum_{i=1}^{N}\sum_{j \neq i} I(X_i)I(X_j)}{\sum_{i=1}^{N}\sum_{j \neq i} |I(X_i)I(X_j)|}, \qquad (2)$$

12

261   where $I(X_i)$ corresponds to the imaginary component of time series data (X) from channel i.

262   Specifically, dwPLI is the sum of all pairwise products of the magnitudes of the imaginary

263   components. In addition, dwPLI accounts for any bias due to the number of data points.

264

265   *2.5 dMRI Acquisition and Preprocessing*

266   Diffusion spectrum imaging (DSI) scans were acquired for each session. DSI scans

267   sampled 258 directions using a Q5 half-shell acquisition scheme with a maximum b-value of

268   5,000 and an isotropic voxel size of 2.4 mm. Minimal preprocessing was carried out on the DSI

269   scans and was restricted to motion correction. Following a similar procedure to the fMRI motion

270   correction, motion was first assessed and applied for all of the b0 volumes, and a template was

271   created for each scan composed of the average of the b0 volumes. Next, the b0 volumes and

272   vectors were transformed using the estimated head motion correction, b0 template coregistration,

273   b0 template-to-T1w coregistration and spatial normalization into MNI space using a single

274   Hamming weighted sinc interpolation.

275   Fiber tracking was performed in DSI Studio (www.dsi-studio.labsolver.org) with an

276   angular cutoff of 35°, step size of 1.0 mm, minimum length of 10 mm, spin density function

277   smoothing of 0, and a maximum length of 250 mm. Deterministic fiber tracking was performed

278   until 500,000 streamlines were reconstructed for each session. As with the fMRI volume data,

279   streamline counts were estimated in 200 nodes using the same Schaefer 200 atlas (Schaefer et al.,

280   2018) and 21 subcortical regions part of the Harvard-Oxford atlas (Makris et al., 2006).

281   Connectivity matrices were then normalized by dividing the number of streamlines (T) between

282   region i and j, by the combined volumes (v) of region i and j,

283     $$A_{ij} = \frac{T_{ij}}{v_i + v_j}. \qquad (3)$$

13

284 *2.6 Graph Theoretical Analysis*

285   We calculated nine commonly used and diverse graph metrics on each weighted dMRI,

286 fMRI and EEG network. The graph metrics are: degree, clustering coefficient, characteristic path

287 length, small-world propensity, global and local efficiency, synchronizability, spectral radius,

288 and eigenvector centrality. See supplemental for detailed description of each network measure.

289 *2.7 Degree*

290   The weighted node degree (k_i) is defined as the sum of all connections of a node

291 (Rubinov and Sporns, 2010),

292
$$k_i = \sum_{j \in N} W_{ij}, \quad (4)$$

293 where W is the weighted adjacency matrix of a network with N nodes.

294

295 *2.8 Clustering Coefficient*

296   The weighted clustering coefficient (C) for node i is the intensity of triangles in a

297 network (Onnela et al., 2005) and is calculated as,

298

299
$$C_i = \frac{1}{b_i(b_i-1)} \sum_{j,h} (W_{ij} \, W_{ih} \, W_{jh})^{1/3}, \quad (5)$$

300 where W is the weighted adjacency matrix and b is the number of edges for node i.

301

302 *2.9 Characteristic Path Length*

303   The characteristic path length (L) is the average shortest path length between all nodes

304 (Rubinov and Sporns, 2010),

14

305
$$L = \frac{1}{N} \sum_{i \in N} \frac{\sum_{j \in N, j \neq i} d_{ij}^{W}}{N-1}, \quad (6)$$

306   where d_{ij}^{W} is the is the distance between nodes i and j. To calculate d_{ij}^{W} , we first take the inverse

307   of the edge weights to transform the weight to a measure of length (i.e., to transform a strong

308   connection strength to a short length). We then determine the shortest path between nodes i and j

309   (using the inverted weights), and d_{ij}^{W} is the sum of the inverse of the edge weights along this

310   shortest path.

311

312   *2.10 Small-World Propensity*

313   Small-world propensity (φ) quantifies the extent to which a network displays small-

314   worldness, a network property that combines the presence of local clustering with a short path

315   length, while factoring in variation in network density (Muldoon et al., 2016). Small-worldness

316   is calculated as,

317
$$\phi = 1 - \sqrt{\frac{\Delta_C^2 + \Delta_L^2}{2}}, \quad (7)$$

318

319
$$\Delta_C = \frac{C_{latt} - C_{obs}}{C_{latt} - C_{rand}}, \quad (8)$$

320

321
$$\Delta_L = \frac{L_{obs} - L_{rand}}{L_{latt} - L_{rand}}, \quad (9)$$

15

322 where C_{obs} is the observed clustering coefficient and L_{obs} is the observed characteristic path

323 length of the network; C_{latt}, L_{latt}, C_{rand}, and L_{rand} are clustering coefficient and characteristic path

324 length from lattice and random networks with the same number of nodes and edge distribution.

325

326 *2.11 Global and Local Efficiency*

327   The efficiency of a node is the inverse of the path length (Rubinov and Sporns, 2010).

328 Global efficiency (E_g) is the inverse shortest path length,

329
$$E_g = \frac{1}{N} \sum_{i \in N} \frac{\sum_{j \in N, j \neq i} (d_{ij}^W)^{-1}}{N-1} , \qquad (10)$$

330 where d_{ij}^W is the previously defined distance between node i and j.

331

332 Local efficiency (E_l) is the global efficiency computed on the neighborhood of node i,

333
$$E_l = \frac{1}{N} \sum_{i \in N} \frac{\sum_{j,h \in N, j \neq i} (w_{ij} w_{ih} [d_{jh}^W (N_i)]^{-1})^{1/3}}{k_i (k_i - 1)} , \qquad (11)$$

334 where w_{ij} and w_{ih} is strength of the connection between node i to j and h, respectively, and d_{jh}

335 *(Ni)* is the length of the shortest path between nodes j and h that contains only neighbors of node

336 *i*.

337

338 *2.12 Synchronizability*

339   Synchronizability is a measure of linear stability for a network of coupled dynamical

340 systems (Motter et al., 2005),

341
$$S = \frac{\lambda_2}{\lambda_n} , \qquad (12)$$

342   where λ_2 is the second smallest eigenvalue of the unnormalized Laplacian matrix (L) and λ_n is its

343   largest eigenvalue. The Laplacian is calculated as,

$$L = D - W, \qquad (13)$$

345   where D is the degree matrix of the weighted adjacency matrix, W.

346

347   *2.13 Spectral Radius*

348   The spectral radius measures the ease with which diffusion process can occur in a

349   network. The spectral radius is calculated as,

$$\rho(W) = \max\{|\lambda_1|, \dots, |\lambda_n|\}, \qquad (14)$$

351   where $|\lambda|$ corresponds to the absolute value of the eigenvalues of a network.

352

353   *2.14 Eigenvector Centrality*

354   Eigenvector centrality (EC_i) measures how influential a node is in a network, with a high

355   value indicating a node is connected to other highly influential nodes (Newman, 2008). The

356   eigenvector centrality of node i is given by the i-th entry in the dominant eigenvector, which is

357   the vector $v=[v_1,\dots v_N]$ that solves

$$\lambda_1 v = W v^T, \qquad (15)$$

359   where λ_1 is the largest eigenvalue of the weighted adjacency matrix, W.

360

361   *2.15 Intra-class Correlation*

362   The intra-class correlation (ICC) is a measure used to quantify the test-retest reliability of

363   a measure. We used the ICC to measure the consistency of individual connections across the

17

364   dMRI, fMRI and EEG networks and across the graph metrics for each network. To accomplish

365   this, we calculated two variants of the ICC, the within (ICC_w)- and between (ICC_b)-subjects (Wei

366   et al., 2004). ICC_w and ICC_b are, respectively, calculated as,

367

368
$$ICC_w = \frac{I(RMS-EMS)}{J*SMS+I*RMS+(IJ-I-J)EMS} , \qquad (16)$$

369

370
$$ICC_b = \frac{J(SMS-EMS)}{J*SMS+I*RMS\ (IJ-I-J)EMS} , \qquad (17)$$

371

372   where I is the number of subjects and J is the number of sessions, *SMS, RMS and EMS* represent

373   the ANOVA measures of mean square error between sessions, subjects, and due to error,

374   respectively. The reliability of a measurement is considered: 1) "poor" if the ICC values is less

375   than 0.4; 2) "fair" for ICC values between 0.4 and 0.6; 3) "good" for ICC values between 0.6 and

376   0.8; and 4) "excellent if ICC values exceed 0.8.

377

378   *2.16 Fingerprinting Analysis*

379   To perform a fingerprinting analysis, as in Finn *et al.*, 2015, we quantified the degree of

380   similarity between networks. This analysis was performed separately for each of the dMRI,

381   fMRI and EEG modalities. Connectivity matrices were converted for each individual and run

382   into a vector using the values from the upper triangle of the matrix resulting in vectors of 1 x

383   24,310 for dMRI and fMRI, and 1x 2,016 for EEG. Thus each vector, *p*, represents a single

384   connectivity matrix for a given subject during a given session, and for functional matrices, in a

385   given state (task/rest).

386   Next, separately within each modality, for each connectivity matrix (representing a

387   subject, session, and state), we calculated the pairwise similarity between two vectors, p and q,

388   using the Euclidian distance to create a dis-similarity matrix (D) where

389

390

391
$$D_{pq} = \sqrt{\Sigma(p-q)^2}\,, \qquad (18)$$

392   and each entry in D_{pq}, corresponds to the dis-similarity between the brain network p to q.

393   However, since the Euclidian distance formally assesses dis-similarity and we were interested in

394   evaluating similarity, we converted from a dis-similarity to a similarity (S) measure by

395

396
$$S_{pq} = \frac{max(D)-D_{pq}}{max(D)}\,, \qquad (19)$$

397   where *max(D)* corresponds to the largest value in matrix D. This normalization ensures that the

398   similarity matrix $S \in [0\ 1]$.

399   In order to perform a fingerprinting analysis, for each vector, p, we then looked for the

400   entry S_{pq} with the highest similarity value. If for this entry, the vectors p and q were from the

401   same individual (but could be from different sessions or states), then the fingerprinting analysis

402   was classified to be successful at identifying the individual.

403   Fingerprinting performance for each imaging modality was assessed using two measures.

404   The first measure quantifies the overall fingerprinting accuracy across subjects, and was

405   calculated as the percentage of matrices which were successful in identifying an individual.

406   While this measure is useful from a classification standpoint, we were also interested in the level

407   of separation between matrices within versus between individuals. Therefore, in the second

19

408   measure, we assessed the separability (T) of each modality. The separability of each matrix, T_p,

409   was defined to be

410    $$T_p = \min_{within-subject}\{S_{pq}\} - \max_{between-subject}\{S_{pq}\}, \qquad (20)$$

411   where the first term is constrained to q from the same subject as p, and the second term is

412   constrained to q from all subjects other than p. The resulting values of $T \in [\text{-1 } 1]$, where a value

413   of 1 indicates perfect similarity within a subject across sessions and no similarity to other

414   subjects and, conversely, -1 indicates no similarity across runs within a subject.

415

416   *2.17 Statistical Tests*

417   Analysis of variance (ANOVA) was used to quantify the magnitude difference in ICC

418   scores and the difference in the magnitude of the network similarity. Corresponding p-values

419   were corrected for multiple comparison using Boneferroni correction. The Brain Connectivity

420   Toolbox was used to calculate network measures (Rubinov and Sporns, 2010). All analyses were

421   conducted in MATLAB 2017b.

422

423   **3 Results**

424   We analyzed the reproducibility of brain network properties derived from structural and

425   functional brain imaging using the intra-class correlation (*ICC*). For the dMRI analysis, this

426   involved analyzing brain networks from 25 subjects across 8 sessions for a total of 200 structural

427   networks. For the fMRI and EEG analysis, a tradeoff between maximizing subjects and sessions

428   was made across resting-state and tasks resulting in a range from 17-26 subjects, each with 6

429   sessions (see Methods section for details).

430

20

431   *3.1 Reliability of Individual Connections*

432   We first assessed the reliability of individual connections between brain regions or

433   sensors. We calculated the ICC within a subject (ICC_w) and between subjects (ICC_b) for each

434   connection across the three imaging modalities. As expected, we found that across imaging

435   modalities, individual network connections are more reliable within- than between-subjects

436   (Figure 1A and B). Across imaging modalities, individual edges exhibit high variability in their

437   reliability scores, with ICC_w values ranging from poor (< 0.4) to excellent (> 0.8) reliability

438   (Figure 1A). By contrast, ICC_b scores had consistently poor (< 0.2) reliability across all imaging

439   modalities (Figure 1B). For dMRI, the mean ICC_w was 0.21 ± 0.24 (SD) and the mean ICC_b

440   score was $-1 \times 10^{-4} \pm 0.01$ (SD). For resting-state fMRI the mean ICC_w was $0.23 + 0.13$(SD).

441   Lastly, for the EEG the α-band had the highest mean ICC_w ($0.39 + 0.16$(SD) compared to the

442   other frequencies (δ: 0.03 ± 0.05(SD); θ: 0.09 ± 0.08(SD); β: 0.20 ± 0.12(SD); γ: $0.10 \pm$

443   0.07(SD)). An ANOVA assessing differences across imaging modalities found significant

444   differences in the ICCw ($F_{6,85249} = 2241$; $p_{corrected} \ll 0.001$). One important feature is the long-

445   tail distribution in the dMRI ICC_w indicating that a small number of connections have excellent

446   (> 0.8) reliability. We additionally looked to see if there was a relationship between connection

447   strength and reliability (Figure 1C-E).

448
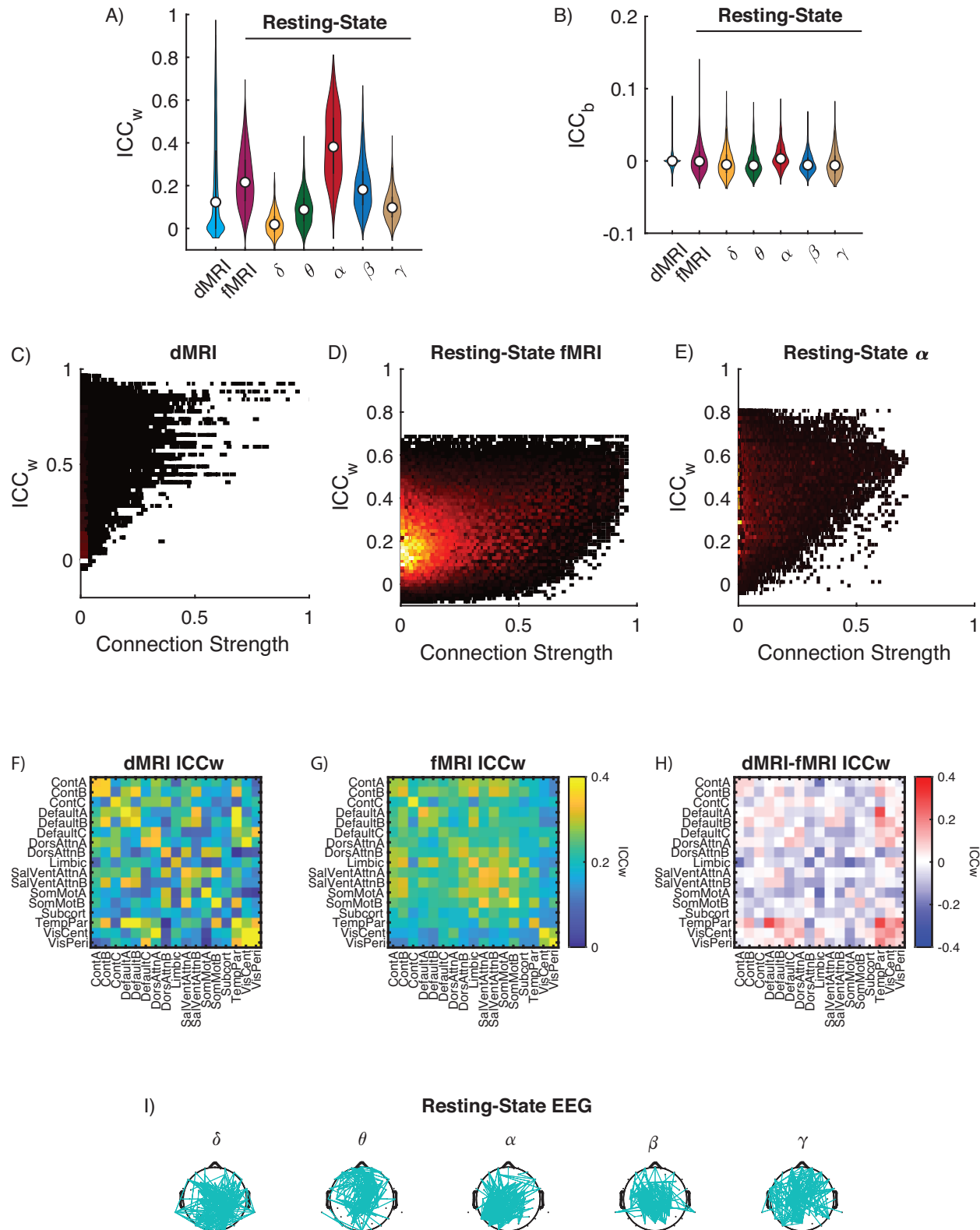
Figure 1. Reliability of individual connections. (A) Distribution of ICC_w and (B) ICC_b for dMRI and resting-state fMRI and EEG frequency bands. For each violin plot, the central dot indicates the median, and the line indicates the 25th to 75th percentiles. (C-E) Cumulative distribution

453 plots showing the proportion of connections and corresponding connection strength from the top
454 10% (most reliable) and bottom 10% (least reliable) of ICC_w scores for (C) dMRI; Resting-State
455 (D) fMRI and (E) EEG-α. F-H) Average reliability of connection within and between cognitive
456 systems for (F) dMRI and (G) resting-state fMRI. H) Differences in average ICC_w scores across
457 cognitive systems between dMRI minus the fMRI. (I) Connections with ICC_w scores in top 10%
458 for δ , θ, α, β and γ frequency bands plotted on the scalp for resting-state EEG. Cognitive
459 systems are defined as Cont: Control A/B/C, Default: Default Mode A/B/C, DorsAttn: Dorsal
460 Attention A/B, Limbic, SalVentAtt: Salience/Ventral Attention A/B, SomMot: Somatomotor
461 A/B, Subcortical, TempPar: Temporal Parietal, VisCent: Visual Central, VisPer: Visual
462 Peripheral.
463

464 We next assessed if for dMRI and resting-state fMRI there is an association between

465 ICC_w scores and cognitive systems. First, we mapped edgewise scores and then averaged over

466 edges within each of the 17 cognitive systems from the Schaefer 200 layout combined with 21

467 subcortical regions from Harvard-Oxford atlas. As a trend, connections within a cognitive system

468 for dMRI and resting-state fMRI exhibited the strongest reliability as can be seen from the figure

469 because of the high values along the diagonal (Figure 1F and G, respectively). However, a direct

470 comparison between dMRI and fMRI showed distinct distribution of reliability across cognitive

471 systems. dMRI reliability was stronger within the Frontal-Parietal Control system and between

472 the Visual, Default Mode, and Temporal Parietal systems (red entries in Figure 1H), while in

473 fMRI, stronger values were distributed between cognitive systems (blue entries in Figure 1H).

474 For the EEG data we could not perform the same mapping to cognitive systems, so instead

475 resting-state ICC_w scores from the top 10% ICCw distribution are plotted onto the scalp (Figure

476 1I).

477 Given the different cognitive demands associated with task performance, one might

478 expect reliability scores during task states to differ from those at rest. However, when we

479 examined task induced changes in reliability, we found that task associated ICC_w and ICC_b

480 values for fMRI and EEG scores exhibited similar pattern to resting-state (Figures 2 and 3,

23

481 respectively). To test for changes, we assessed an ICC x Task ANOVA and found that the ICC x

482 Task interaction was significant ($F_{10,501389}$ = 1242, $p_{corrected}$ << 0.001). For the EEG, we

483 additionally added frequency as a variable in our ANOVA design and found that the ICC x Task

484 x Frequency interaction was significant ($F_{40, 201190}$ = 140, $p_{corrected}$ << 0.001) with the α-band

485 having the highest ICC_w scores.
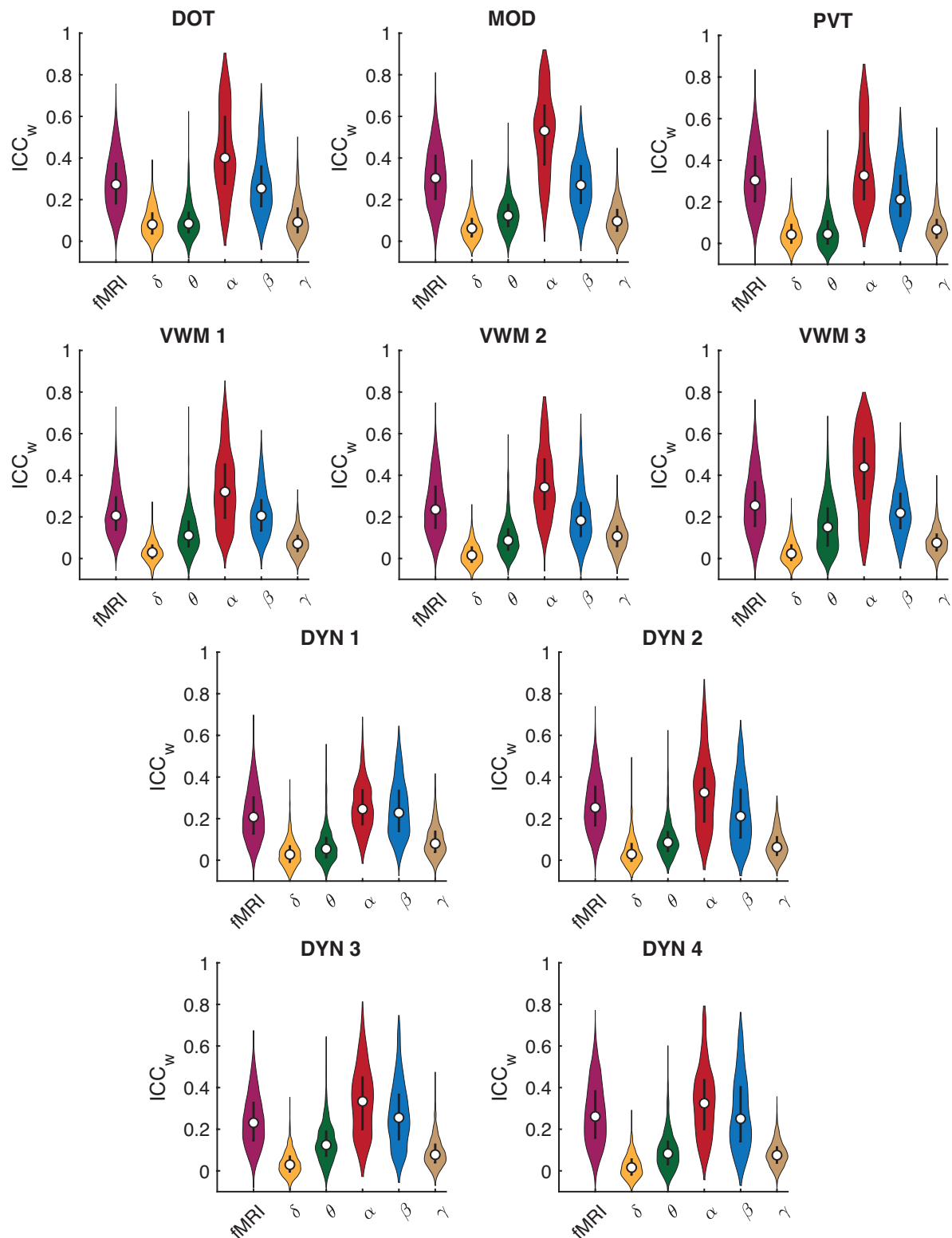
Figure 2. Reliability of individual connections within-subjects (ICC_w) for fMRI and EEG frequency bands across tasks: DOT, PVT, MOD, VWM-1:3, and DYN-1:4. For each violin plot, the central dot indicates the median, and the line indicates the 25th to 75th percentiles. DOT: Dot

490   Probe Task; DYN: Dynamic Attention Task; MOD: Modular Math Task; PVT: Psychomotor
491   Vigilance Task; VWM 1-3: Visual Working Memory.
492
493
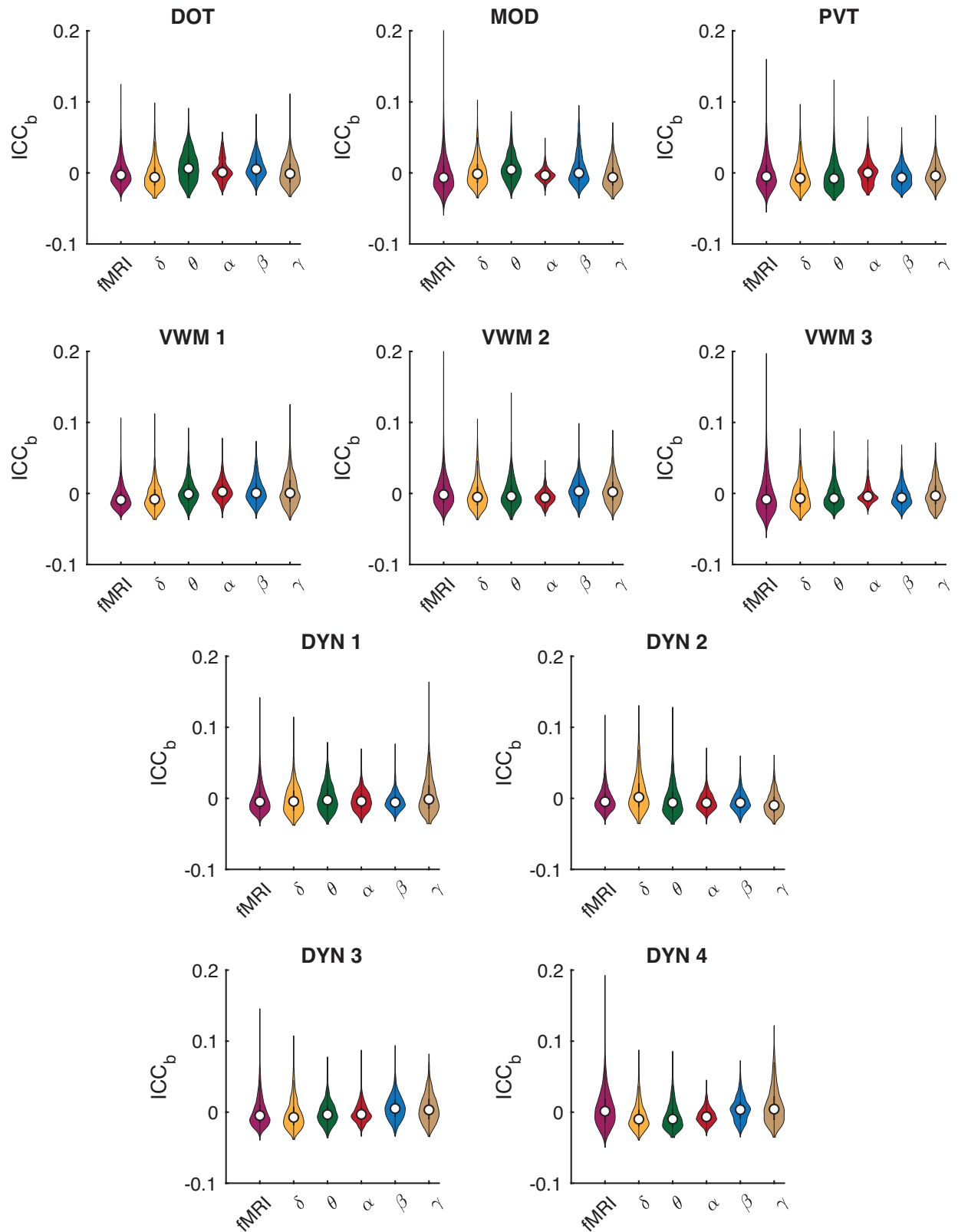
Figure 3. Reliability of individual connections between-subjects (ICC_b) for fMRI and EEG frequency bands across tasks: DOT, PVT, MOD, VWM-1:3, and DYN-1:4. For each violin plot, the central dot indicates the median, and the line indicates the 25th to 75th percentiles. DOT: Dot

498 Probe Task; DYN: Dynamic Attention Task; MOD: Modular Math Task; PVT: Psychomotor
499 Vigilance Task; VWM 1-3: Visual Working Memory.
500
501

502   Similarly, we assessed if for task fMRI there is an association between ICC_w scores and

503 cognitive systems. We mapped edgewise scores to the 17 cognitive systems in the same manner

504 as for the resting-state and plotted the difference between the ICC_w values during task and

505 resting-state in Figure 4. We generally observed higher reliability during task states, and found

506 that for tasks with repeated sessions, the ICC_w progressively increased from resting-state as the

507 sessions progressed (Figure 4 VWM and DYN tasks). For task EEG data, ICC_w scores from the

508 top 10% of the ICC_w distribution were plotted onto the scalp and we did not notice any overt

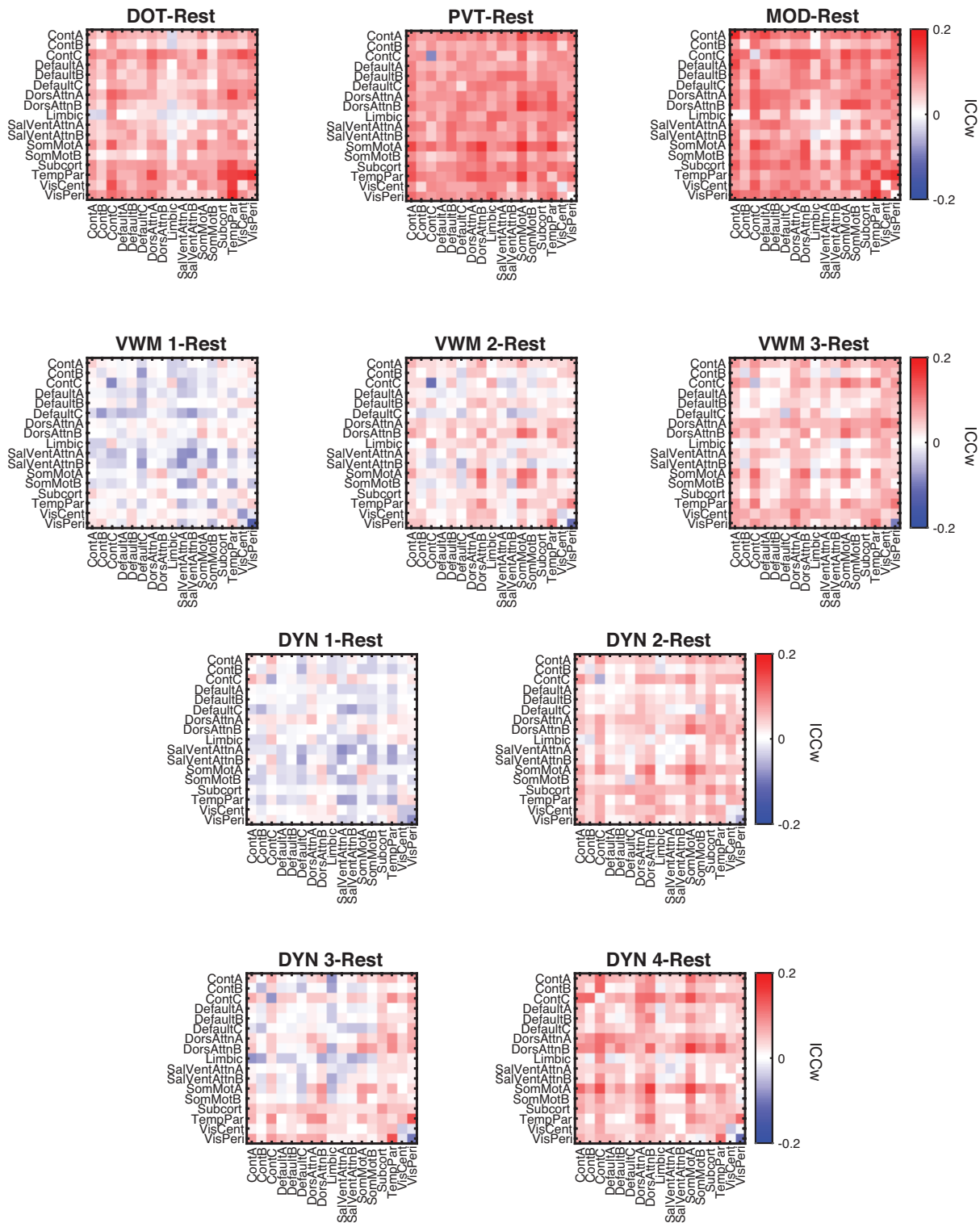509 reconfiguration in scalp distribution from resting-state to task (Figure 5).

510

511

512

513
514
515

28

Figure 4. fMRI changes in reliability from resting-state for each task: DOT, PVT, MOD, VWM-1:3, and DYN-1:4. Connections are mapped unto 17 cognitive systems from Schaefer cortical and Harvard-Oxford subcortical atlas. DOT: Dot Probe Task; DYN: Dynamic Attention Task;

522 MOD: Modular Math Task; PVT: Psychomotor Vigilance Task; VWM 1-3: Visual Working
523 Memory.

524
525
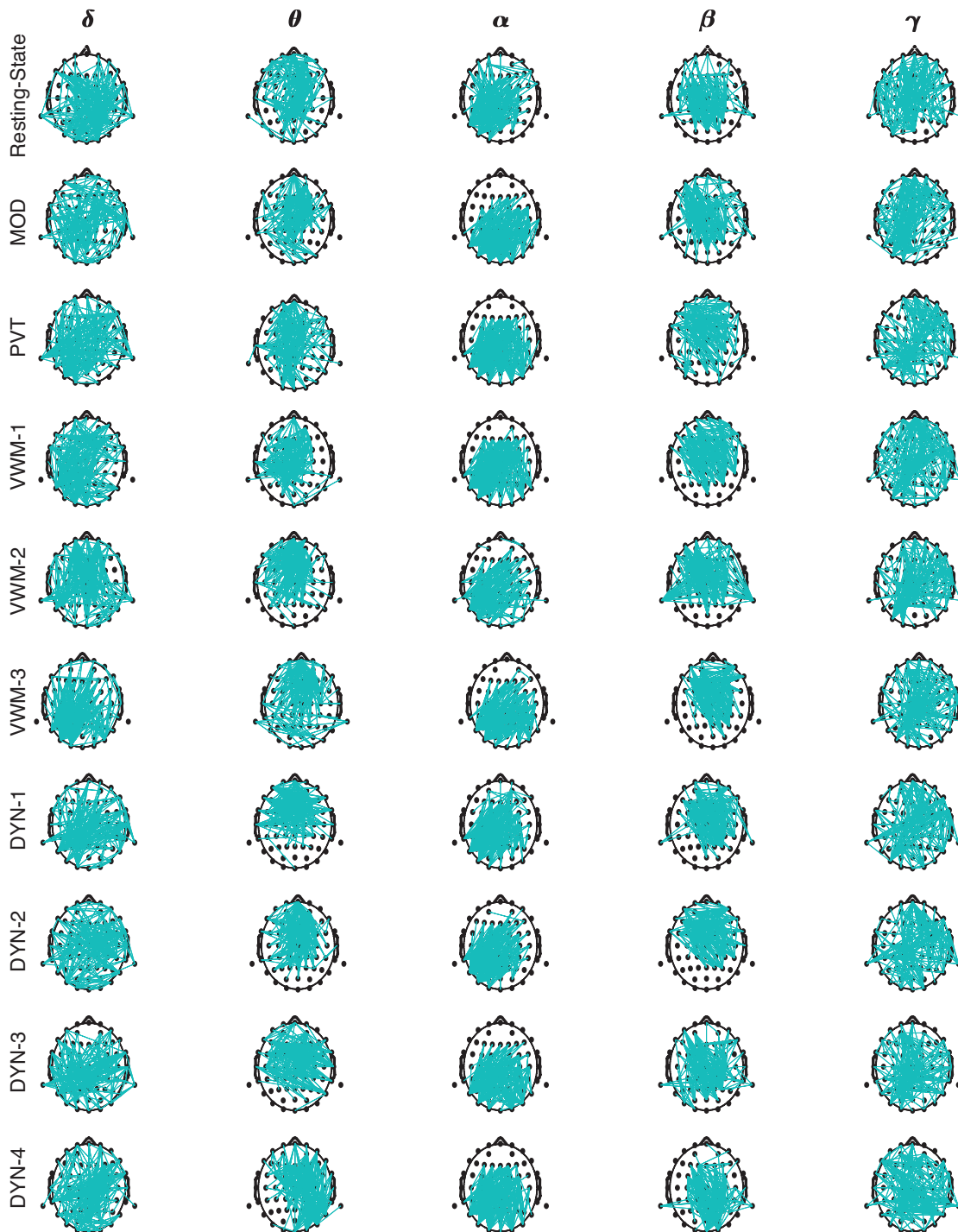
526
527
528 **Figure 5.** Scalp distribution across tasks for top 10% of ICC$_w$ scores. For Resting-State and each
529 task: DOT, PVT, MOD, VWM-1:3, and DYN-1:4, (10 in total), connections with ICC$_w$ scores in
530 top 10% for δ , θ, α, β and γ frequency bands are plotted on the scalp. DOT: Dot Probe Task;

30

531 DYN: Dynamic Attention Task; MOD: Modular Math Task; PVT: Psychomotor Vigilance Task;
532 VWM 1-3: Visual Working Memory.
533

534 *3.2 Reliability of Network Measures*

535 We next assessed the reliability of higher order network properties. For each brain

536 network, nine measures were calculated along with their corresponding ICC_w and ICC_b scores.

537 We found significant differences between modalities in ICC_w ($F_{6,66}$ = 45; p-corrected << 0.001).

538 As shown in Figure 6 A, across all imaging modalities and network properties, the dMRI

539 exhibited the highest ICC_w scores (0.71 ± 0.06 (SD)) . By comparison, resting-state fMRI

540 exhibited relatively poor reproducibility (0.35 ± 0.12 (SD)), and EEG's reproducibility was

541 frequency dependent with the α-band having the highest ICC_w scores (0.43 ± 0.09 (SD)). ICC_b

542 scores across all modalities were close to zero (Figure 6B).

543
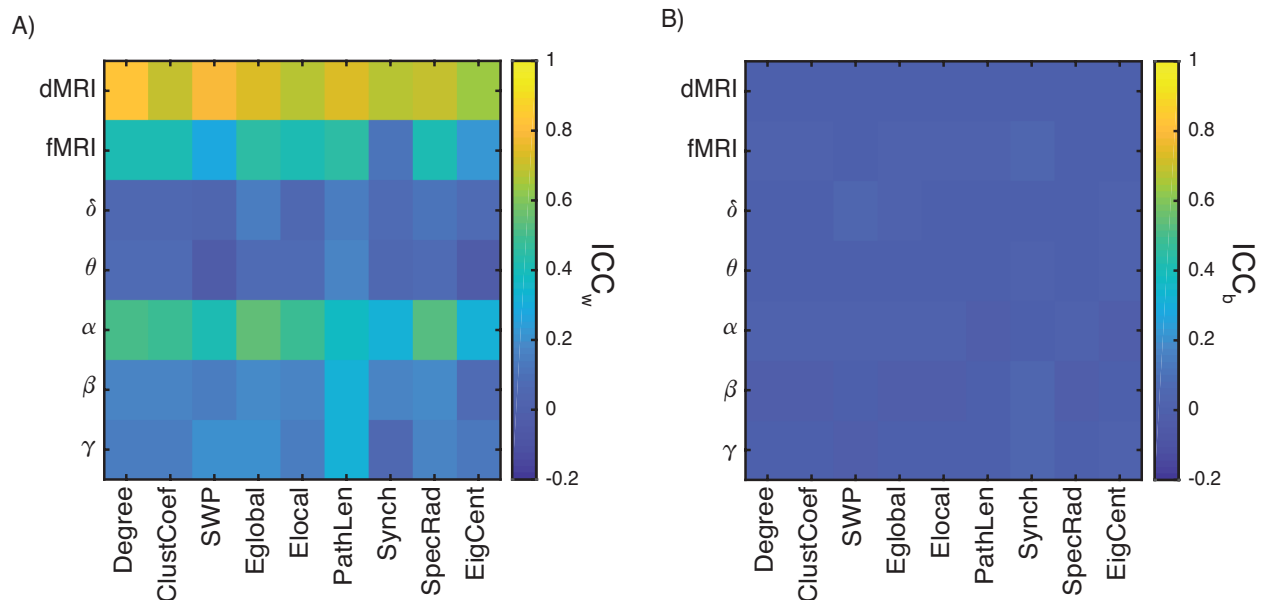
544
545

546 **Figure 6.** Graph Measures for dMRI and Resting-State fMRI and EEG for (A) ICC_w and (B)
547 ICC_b values.
548

549   We next assessed if performing a task alters the reliability of network measures (Figure

550   7). For fMRI, we evaluated the Task x Network Measure x ICC ANOVA design and found

551   significant interactions between Task x ICC ($F_{8,80} = 99$, $p_{corrected} \ll 0.001$) and Network Measure

552   x ICC ($F_{10,80} = 9.88$, $p_{corrected} \ll 0.001$) (Figure 7A). For the EEG, we evaluated the Task x

553   Frequency x Network Measure x ICC ANOVA design, and we found a significant interaction

554   between Task x Frequency ($F_{32,792} = 5.35$, $p_{corrected} < 0.001$) and Frequency x Network Measure

555   ($F_{40,792} = 6.33$, $p_{corrected} < 0.001$) (Figure 7A). From Figure 7 it is apparent that the α-band is the

556   most consistent across resting- and task-state, while the β-band shows an increase in ICC_w in the

557   task-states. It is also worth noting that Synchronizability and Eigenvector Centrality exhibited

558   weaker ICC_w scores relative to the other metrics across resting- and task-states for both fMRI

559   and EEG.
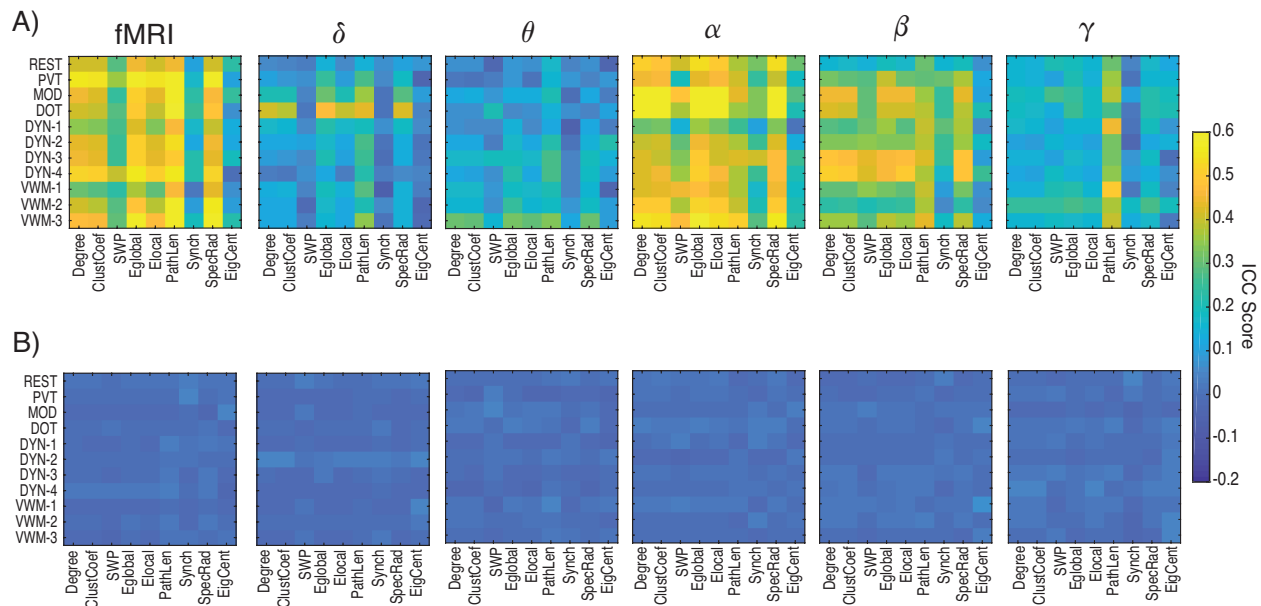
560

561   **Figure 7.** ICC values for network measures across task and resting-state. (A) ICC_w and (B) ICC_b
562   values across tasks for fMRI and EEG frequency bands.
563

564   *3.3 Fingerprinting Analysis*

565   Our analysis so far has confirmed that dMRI networks are more reliable within a subject

566   than fMRI and EEG networks. We therefore, expect that dMRI networks will have a higher

567   probability of being able to identify an individual from a group, similar to a fingerprint (Finn et

568   al., 2015). For functional networks, we would similarly expect the same of α-band EEG

569   networks, given their relatively higher reliability scores. In order to fingerprint an individual,

570   brain networks from the individual should be more similar to each other across runs relative to

571   networks obtained from other individuals. To formally assess the similarity between brain

572   networks, we measured similarity using the Euclidian distance (Methods). Our results indicate

573   that fingerprinting was not uniform across all derived networks ($F_{6,168} = 3402$, $p_{corrected} \ll 0.001$).

574   As expected, structural dMRI networks had the highest accuracy, but for functional networks,

575   fMRI networks performed better than α-band EEG derived networks, and in fact, within EEG

576   networks, β-band networks had the highest fingerprinting accuracy (Figure 8A).

577
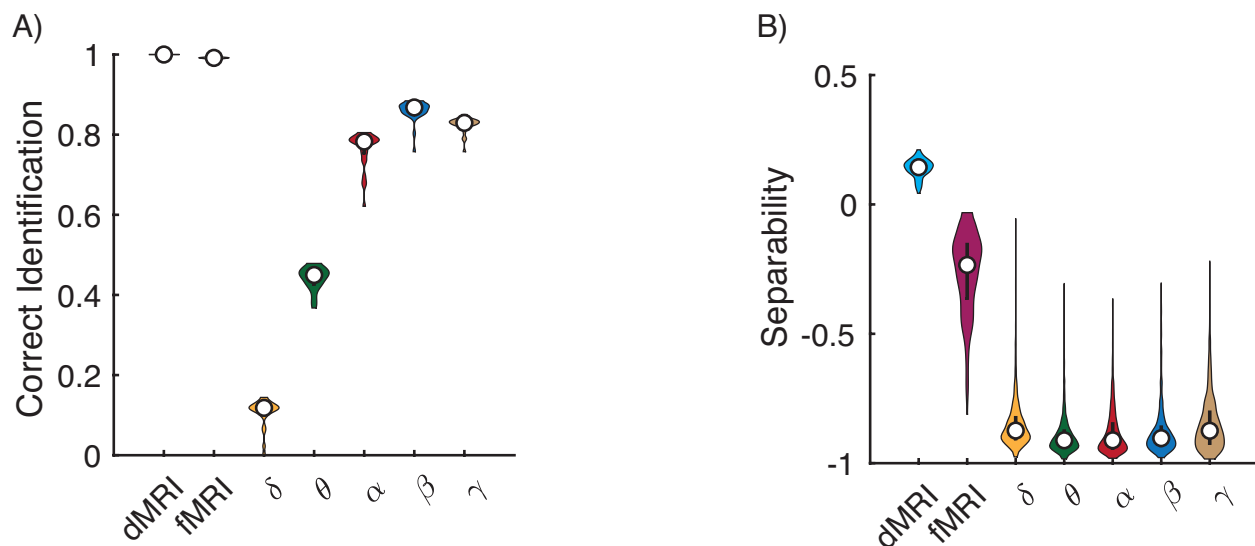
578

579   **Figure 8.** Fingerprinting performance across imaging modalities. (A) Proportion of networks
580   that were correctly matched to the corresponding individual for dMRI, fMRI, and EEG derived
581   brain networks. (B) Separability of each network in being matched to corresponding individual.
582   For each violin plot, the central dot indicates the median, and the line indicates the 25th to 75th

583   percentiles.

584

585   However, this analysis does not tell us about the separability across the networks derived

586   from the different imaging modalities. Here we define separability as the difference in similarity

587   between the minimum within-subject value for a network to the maximum between subject

588   similarity for that network (Methods). Therefore, positive separability values indicate that a

589   particular network for an individual is always more similar to other networks from that

590   individual and negative values indicate the opposite. Separability values across imaging

591   modalities were found to be significantly different ($F_{6,10093} = 8618$; $p_{corrected} \ll 0.001$). In

592   addition, despite dMRI and fMRI having similar accuracy in fingerprinting, dMRI networks

593   were more separable than fMRI and EEG (dMRI: 0.14 ± 0.04 (SD); fMRI: -0.26 ± 0.27 (SD); δ ,

594   θ, α, β and γ: < -0.85 (mean)) (Figure 8B).

595

596   **4 Discussion**

597   In the current work, we analyzed the reproducibility of multimodal and multi-task

598   structural and functional brain networks in a unique longitudinal and multi-modal data set with

599   simultaneous EEG-fMRI recordings. In our analysis, each subject contained brain networks

600   derived from dMRI, fMRI and EEG data, allowing us to assess how reliability differed in brain

601   networks derived from different modalities and across task states.

602

603   *4.1 Edgewise Reliability Differences Between dMRI, fMRI, and EEG*

604   We first assessed the reliability of individual connections in the structural and functional

605   brain networks and found stronger within- than between-subject reliability across all imaging

606   modalities, in line with previous results (Birn et al., 2013; Noble et al., 2019, 2017; O'Connor et

607   al., 2017; Pannunzi et al., 2017; Shehzad et al., 2009). The most reliable connections were also

608   the ones that tended to be the strongest, corroborating previous findings in fMRI networks

609   (Noble et al., 2017; Pannunzi et al., 2017). In addition, these connections when mapped on to

610   cognitive systems, exhibited distinct patterning. As a trend, for dMRI and resting-state fMRI,

611   connections within a cognitive system exhibited the strongest reliability, consistent with previous

612   studies in functional networks (Birn et al., 2013; Noble et al., 2017; O'Connor et al., 2017;

613   Shehzad et al., 2009). However, a direct comparison between dMRI and resting-state fMRI

614   showed distinct distribution of reliability across cognitive systems. dMRI reliability was

615   strongest within the Frontal-Parietal Control system and between the Visual to Default Mode and

616   Temporal Parietal system, while in resting-state fMRI stronger values were distributed between

617   cognitive systems.

618   When assessing task mediated changes, we found an increase in reliability across most

619   tasks relative to resting-state in fMRI networks. In addition, we observed an increase in this

620   reliability across multiple sessions of a given task, potentially indicative of an effect of learning

621   the task. This finding compliments results from a previous study that found adding task-state

622   fMRI networks improves predictive outcomes relative to resting-states fMRI (Gao et al., 2019).

623   For EEG, the α- and β-bands had the highest reliability scores for both resting- and task-

624   states, confirming previous results (Kuntzelman and Miskovic, 2017). The strong reliability for

625   the α- and β-band could be due to the fact that these frequencies are consistently activity, while

626   the other frequency bands tend to have transient activity. In a similar manner to fMRI, EEG

627   reliability increased during a task, but this increase was primarily in the α- and β-bands. In

628   addition, we found no major changes when we mapped connections on the scalp from resting-

629   state to task-state. This could be due to the low spatial resolution of EEG (Nunez et al., 1997).

630

631   *4.2 Reliability of Graph Theoretical Measures*

632   When examining the reliability of higher order network properties, we found that

633   network properties had overall stronger reliability scores than individual connections in line with

634   previous findings of Braun et al., 2012. This might lead one to ask how the prevalence of low

635   reliability scores across most connections could produce fair to excellent reliability in higher

636   order network properties? This result could be due to the fact that edges with higher reliability

637   scores are associated with the stronger connections. Our graph theoretical properties are

638   dependent on connection strength, and the stronger the connection, the more variance it accounts

639   for in the higher order network values. Thus, despite most connections having poor reliability,

640   the few strong connections with good to excellent reproducibility have a disproportionately

641   higher impact on the reliability of a network measure. The notable exception is that in fMRI and

642   EEG, synchronizability and eigenvector centrality had lower reliability scores than the other

643   network properties. One possible reason for this is that these measures, particularly eigenvector

644   centrality, are very sensitive to the state of the subject (Lohmann et al., 2010). These results

645   indicate these measures might be more sensitive to detecting meaningful differences between

646   individuals in studies where one is attempting to link functional brain connectivity to task

647   performance or behavior.

648   We also found task associated differences in reliability for the fMRI and EEG. However

649   for the EEG, the strongest increases in reliability were in the α- and β-bands. However, in

650   contrast to Deuker *et al.,* 2009 we did not find a corresponding increase in ICC_w scores in the δ

651   and θ bands with task.

652

653

654   *4.3 Fingerprinting*

655   We found that dMRI and fMRI outperformed EEG derived networks in fingerprinting.

656   However, the separability was not equal across these networks, with dMRI outperforming all

657   functional networks. This is likely due to the fact that, unlike functional connectivity, structural

658   connectivity is not state dependent.

659   It has been found that brain activity measured with fMRI is stable over time (Braga and

660   Buckner, 2017; Gratton et al., 2018; Horien et al., 2019; Laumann et al., 2015) and in fMRI,

661   within-subject variance can be reduced with high quality data with long scan times (~15 minutes)

662   and multiple sessions (Birn et al., 2013; Laumann et al., 2015; Noble et al., 2017; Pannunzi et al.,

663   2017). It has been argued that large amounts of data are needed in order to differentiate between

664   true and artifact induced variance (Gordon et al., 2017; Power et al., 2012) and previous studies

665   have found that reliability increases with more data (Anderson et al., 2011; Birn et al., 2013;

666   Laumann et al., 2015; Noble et al., 2017; Shou et al., 2013). This high quality data is important

667   because Horien *et al.*, 2019 found that motion characteristics can be unique to an individual and

668   can fingerprint a subject at a level greater than chance. In our data, individual scan times were

669   limited to approximately 5 minutes, but data was collected over multiple sessions for a relatively

670   large number of subjects, suggesting that we might expect more reliable results. However, our

671   observation of the relatively weak accuracy and separability of EEG (a more direct measure of

672   neuronal activity than fMRI) in fingerprinting an individual raises questions as to whether the

673   increase in fingerprinting performance in fMRI on long time scans is based on neuronal activity.

674   Also, respiration induced artifacts in fMRI exhibit the same stability over time (Power et al.,

675   2019), which could also lead to increased reliability measurements.

676   Our direct comparison of fingerprinting between structural and functional networks

677   indicates that structural networks more sensitive. In addition, these results indicate that the

678   patterning in structural connectivity is far more unique to an individual than those in

679   corresponding functional networks. These results suggest that structural networks might have

680   more discriminative power than functional networks.

681   Unique brain connectivity features have previously been proposed to play a role in

682   differences underlying behavior and cognition (Kanai and Rees, 2011). Specifically, difference

683   in behavioral performance in motor and decision associated tasks are correlated with fractional

684   anisotropy of the corpus callosum (Johansen-Berg et al., 2007; Westerhausen et al., 2006), optic

685   radiation (Tuch et al., 2005) and grey matter density (Van Gaal et al., 2011). Cortical thickness

686   within the superior parietal lobes has been found to be correlated with the rate of switching in a

687   perception based task (Kanai et al., 2010). In addition structural features unique to an individual

688   lead to characteristic brain functional activity in modeling analysis and task performance (Bansal

689   et al., 2019, 2018a).

690

691   *4.4 On Reliability, Confounding Variables, and Utility*

692   Is a connection with poor reliability good or bad? To answer this, we need to be mindful

693   of the goal at hand. First and foremost, we need to make sure that reliability values are not due to

694   noise in the signal. On the other hand, if we are confident that low reliability is a genuine part of

695   the signal, then that is also a very informative finding. The seminal work of Poldrack et al., 2015

696   found that functional connectivity exhibits a high level of variability within the same person over

697   the course of a year. Along these lines, Noble et al., 2017 found that functional connections with

698   strong reliability are not very informative when it pertains to predicting behavior. However, we

699   need to be mindful that this is an effect limited to functional connectivity. Therefore, structural

700   connections and/or higher-order network metrics might exhibit a stronger association between

701   reliability and behavior. Also, finding highly reproducible brain connections and/or measures

702   might be very important if we are looking for deviations from expected values that could be used

703   as biomarkers for disease identification/progression. Alternatively, connections and/or measures

704   with low reliability might be useful for studying individual differences and making correlations

705   between structure and performance/behavior.

706   But, even beyond reliability and noise, our functional results could, along with previous

707   literature, reflect the natural day-to-day changes in our brain. Neuroplastic changes in the brain

708   are the hallmark of learning and memory (Lamprecht and LeDoux, 2004), and these changes or

709   natural fluctuations and modifications in the *neural code* (Fairhall et al., 2001)*,* reflecting

710   learning and memory could be reflected in functional connectivity. Indeed, there are many

711   examples of rapid neuroplastic changes in the brain that results in functional connectivity

712   changes (e.g., Nierhaus et al., 2019), but see Perich et al., 2018 as an alternative theory.

713   Moreover, in this particular dataset, individuals were recruited to capture substantial variability

714   in sleep without experimental manipulation. While there is a substantial literature on brain

715   related decrements due to sleep deprivation (Boonstra et al., 2007; Hudson et al., 2020) little is

716   known about naturalistic fluctuations in sleep (Moturu et al., 2011; Thurman et al., 2018). These

717   individuals, instead could be more "plastic" (or "stationary") than other individuals. Future

718   studies may disentangle these alternatives from a *reliability* explanation of our results.

719   fMRI-based analysis has been around for over two decades, but its clinical use has been

720   limited, raising questions about its usefulness as a diagnostic tool. In addition, given that the

721   effectiveness of any diagnostic tool is only as useful as it can be applied to an individual, then in

39

722   this regard, structural networks should take a more prominent role in medicine. Regardless, one

723   must consider how measures of reliability relate to the modality being studied, the state of the

724   brain, and the question at hand in order to meaningfully ask questions about how brain networks

725   change with disease or how individual differences in structure relate to performance and

726   behavior.

727

736

References

738   Abraham, A., Pedregosa, F., Eickenberg, M., Gervais, P., Mueller, A., Kossaifi, J., Gramfort, A.,

739   Thirion, B., Varoquaux, G., 2014. Machine learning for neuroimaging with scikit-learn.

740   Front. Neuroinform. https://doi.org/10.3389/fninf.2014.00014

741   Allen, P.J., Josephs, O., Turner, R., 2000. A method for removing imaging artifact from

742   continuous EEG recorded during functional MRI. Neuroimage.

743   https://doi.org/10.1006/nimg.2000.0599

744   Allen, P.J., Polizzi, G., Krakow, K., Fish, D.R., Lemieux, L., 1998. Identification of EEG events

745   in the MR scanner: The problem of pulse artifact and a method for its subtraction.

746   Neuroimage. https://doi.org/10.1006/nimg.1998.0361

747 Amunts, K., Malikovic, A., Mohlberg, H., Schormann, T., Zilles, K., 2000. Brodmann's areas 17

748   and 18 brought into stereotaxic space - Where and how variable? Neuroimage.

749   https://doi.org/10.1006/nimg.1999.0516

750 Anderson, J.S., Ferguson, M.A., Lopez-Larson, M., Yurgelun-Todd, D., 2011. Reproducibility of

751   single-subject functional connectivity measurements. Am. J. Neuroradiol.

752   https://doi.org/10.3174/ajnr.A2330

753 Avants, B.B., Tustison, N.J., Song, G., Gee, J.C., 2009. ANTS: Open-source tools for

754   normalization and neuroanatomy. IEEE Trans. Biomed. Eng.

755   https://doi.org/10.1007/s12021-011-9109-y

756 Bansal, K., Garcia, J.O., Tompson, S.H., Verstynen, T., Vettel, J.M., Muldoon, S.F., 2019.

757   Cognitive chimera states in human brain networks. Sci. Adv.

758   https://doi.org/10.1126/sciadv.aau8535

759 Bansal, K., Medaglia, J.D., Bassett, D.S., Vettel, J.M., Muldoon, S.F., 2018a. Data-driven brain

760   network models differentiate variability across language tasks. PLoS Comput. Biol.

761   https://doi.org/10.1371/journal.pcbi.1006487

762 Bansal, K., Nakuci, J., Muldoon, S.F., 2018b. Personalized brain network models for assessing

763   structure-function relationships. Curr. Opin. Neurobiol. 52, 1–13.

764   https://doi.org/10.1016/J.CONB.2018.04.014

765 Bassett, D.S., Brown, J.A., Deshpande, V., Carlson, J.M., Grafton, S.T., 2011. Conserved and

766   variable architecture of human white matter connectivity. Neuroimage.

767   https://doi.org/10.1016/j.neuroimage.2010.09.006

41

768   Bassett, D.S., Sporns, O., 2017. Network neuroscience. Nat. Neurosci. 20, 353–364.

769   https://doi.org/10.1038/nn.4502

770   Birn, R.M., Molloy, E.K., Patriat, R., Parker, T., Meier, T.B., Kirk, G.R., Nair, V.A., Meyerand,

771   M.E., Prabhakaran, V., 2013. The effect of scan length on the reliability of resting-state

772   fMRI connectivity estimates. Neuroimage.

773   https://doi.org/10.1016/j.neuroimage.2013.05.099

774   Bonilha, L., Gleichgerrcht, E., Fridriksson, J., Breedlove, J.L., Rorden, C., Nesland, T., Paulus,

775   W., Helms, G., Focke, N.K., 2015. Reproducibility of the structural brain connectome

776   derived from diffusion tensor imaging. PLoS One.

777   https://doi.org/10.1371/journal.pone.0135247

778   Boonstra, T.W., Stins, J.F., Daffertshofer, A., Beek, P.J., 2007. Effects of sleep deprivation on

779   neural functioning: An integrative review. Cell. Mol. Life Sci.

780   https://doi.org/10.1007/s00018-007-6457-8

781   Braga, R.M., Buckner, R.L., 2017. Parallel Interdigitated Distributed Networks within the

782   Individual Estimated by Intrinsic Functional Connectivity. Neuron.

783   https://doi.org/10.1016/j.neuron.2017.06.038

784   Braun, U., Plichta, M.M., Esslinger, C., Sauer, C., Haddad, L., Grimm, O., Mier, D., Mohnke, S.,

785   Heinz, A., Erk, S., Walter, H., Seiferth, N., Kirsch, P., Meyer-Lindenberg, A., 2012. Test-

786   retest reliability of resting-state connectivity network characteristics using fMRI and graph

787   theoretical measures. Neuroimage 59, 1404–1412.

788   https://doi.org/10.1016/j.neuroimage.2011.08.044

789   Buchanan, C.R., Pernet, C.R., Gorgolewski, K.J., Storkey, A.J., Bastin, M.E., 2014. Test-retest

790   reliability of structural brain networks from diffusion MRI. Neuroimage.

791   https://doi.org/10.1016/j.neuroimage.2013.09.054

792   Bürgel, U., Amunts, K., Hoemke, L., Mohlberg, H., Gilsbach, J.M., Zilles, K., 2006. White

793   matter fiber tracts of the human brain: Three-dimensional mapping at microscopic

794   resolution, topography and intersubject variability. Neuroimage.

795   https://doi.org/10.1016/j.neuroimage.2005.08.040

796   Chang, C.Y., Hsu, S.H., Pion-Tonachini, L., Jung, T.P., 2020. Evaluation of Artifact Subspace

797   Reconstruction for Automatic Artifact Components Removal in Multi-Channel EEG

798   Recordings. IEEE Trans. Biomed. Eng. https://doi.org/10.1109/TBME.2019.2930186

799   Cieslak, M., Ryan, W.S., Babenko, V., Erro, H., Rathbun, Z.M., Meiring, W., Kelsey, R.M.,

800   Blascovich, J., Grafton, S.T., 2018. Quantifying rapid changes in cardiovascular state with a

801   moving ensemble average. Psychophysiology. https://doi.org/10.1111/psyp.13018

802   Ciric, R., Wolf, D.H., Power, J.D., Roalf, D.R., Baum, G.L., Ruparel, K., Shinohara, R.T.,

803   Elliott, M.A., Eickhoff, S.B., Davatzikos, C., Gur, R.C., Gur, R.E., Bassett, D.S.,

804   Satterthwaite, T.D., 2017. Benchmarking of participant-level confound regression strategies

805   for the control of motion artifact in studies of functional connectivity. Neuroimage.

806   https://doi.org/10.1016/j.neuroimage.2017.03.020

807   Delorme, A., Makeig, S., 2004. EEGLAB: an open source toolbox for analysis of single-trial

808   EEG dynamics including independent component analysis. J. Neurosci. Methods.

809   https://doi.org/10.1016/j.jneumeth.2003.10.009

810   Deuker, L., Bullmore, E.T., Smith, M., Christensen, S., Nathan, P.J., Rockstroh, B., Bassett,

811   D.S., 2009. Reproducibility of graph metrics of human brain functional networks.

812   Neuroimage 47, 1460–8. https://doi.org/10.1016/j.neuroimage.2009.05.035

813   Du, H.X., Liao, X.H., Lin, Q.X., Li, G.S., Chi, Y.Z., Liu, X., Yang, H.Z., Wang, Y., Xia, M.R.,

43

814   2015. Test-Retest Reliability of Graph Metrics in High-resolution Functional

815   Connectomics: A Resting-State Functional MRI Study. CNS Neurosci. Ther.

816   https://doi.org/10.1111/cns.12431

817 Elliott, M.L., Knodt, A.R., Cooke, M., Kim, M.J., Melzer, T.R., Keenan, R., Ireland, D.,

818   Ramrakha, S., Poulton, R., Caspi, A., Moffitt, T.E., Hariri, A.R., 2019. General functional

819   connectivity: Shared features of resting-state and task fMRI drive reliable and heritable

820   individual differences in functional brain networks. Neuroimage 189, 516–532.

821   https://doi.org/10.1016/j.neuroimage.2019.01.068

822 Fairhall, A.L., Lewen, G.D., Bialek, W., De Ruyter van Steveninck, R.R., 2001. Efficiency and

823   ambiguity in an adaptive neural code. Nature. https://doi.org/10.1038/35090500

824 Finn, E.S., Shen, X., Scheinost, D., Rosenberg, M.D., Huang, J., Chun, M.M., Papademetris, X.,

825   Todd Constable, R., 2015. Functional connectome fingerprinting: Identifying individuals

826   based on patterns of brain connectivity HHS Public Access. Nat Neurosci 18, 1664–1671.

827   https://doi.org/10.1038/nn.4135

828 Fornito, A., Zalesky, A., Breakspear, M., 2015. The connectomics of brain disorders. Nat. Rev.

829   Neurosci. 16, 159–172. https://doi.org/10.1038/nrn3901

830 Fox, M.D., Snyder, A.Z., Vincent, J.L., Corbetta, M., Van Essen, D.C., Raichle, M.E., 2005. The

831   human brain is intrinsically organized into dynamic, anticorrelated functional networks.

832   Proc. Natl. Acad. Sci. U. S. A. https://doi.org/10.1073/pnas.0504136102

833 Gao, S., Greene, A.S., Constable, R.T., Scheinost, D., 2019. Combining multiple connectomes

834   improves predictive modeling of phenotypic measures. Neuroimage.

835   https://doi.org/10.1016/j.neuroimage.2019.116038

836 Glover, G.H., Li, T.Q., Ress, D., 2000. Image-based method for retrospective correction of

837   physiological motion effects in fMRI: RETROICOR. Magn. Reson. Med.

838   https://doi.org/10.1002/1522-2594(200007)44:1<162::AID-MRM23>3.0.CO;2-E

839   Gordon, E.M., Laumann, T.O., Gilmore, A.W., Newbold, D.J., Greene, D.J., Berg, J.J., Ortega,

840   M., Hoyt-Drazen, C., Gratton, C., Sun, H., Hampton, J.M., Coalson, R.S., Nguyen, A.L.,

841   McDermott, K.B., Shimony, J.S., Snyder, A.Z., Schlaggar, B.L., Petersen, S.E., Nelson,

842   S.M., Dosenbach, N.U.F., 2017. Precision Functional Mapping of Individual Human Brains.

843   Neuron. https://doi.org/10.1016/j.neuron.2017.07.011

844   Gratton, C., Laumann, T.O., Nielsen, A.N., Greene, D.J., Gordon, E.M., Gilmore, A.W., Nelson,

845   S.M., Coalson, R.S., Snyder, A.Z., Schlaggar, B.L., Dosenbach, N.U.F., Petersen, S.E.,

846   2018. Functional Brain Networks Are Dominated by Stable Group and Individual Factors,

847   Not Cognitive or Daily Variation. Neuron. https://doi.org/10.1016/j.neuron.2018.03.035

848   Hardmeier, M., Hatz, F., Bousleiman, H., Schindler, C., Stam, C.J., Fuhr, P., 2014.

849   Reproducibility of functional connectivity and graph measures based on the phase lag index

850   (PLI) and weighted phase lag index (wPLI) derived from high resolution EEG. PLoS One.

851   https://doi.org/10.1371/journal.pone.0108648

852   Horien, C., Shen, X., Scheinost, D., Constable, R.T., 2019. The individual functional

853   connectome is unique and stable over months to years. Neuroimage.

854   https://doi.org/10.1016/j.neuroimage.2019.02.002

855   Hudson, A.N., Van Dongen, H.P.A., Honn, K.A., 2020. Sleep deprivation, vigilant attention, and

856   brain function: a review. Neuropsychopharmacology. https://doi.org/10.1038/s41386-019-

857   0432-6

858   Johansen-Berg, H., Della-Maggiore, V., Behrens, T.E.J., Smith, S.M., Paus, T., 2007. Integrity

859   of white matter in the corpus callosum correlates with bimanual co-ordination skills.

860   Neuroimage. https://doi.org/10.1016/j.neuroimage.2007.03.041

861   Kanai, R., Bahrami, B., Rees, G., 2010. Human parietal cortex structure predicts individual

862   differences in perceptual rivalry. Curr. Biol. https://doi.org/10.1016/j.cub.2010.07.027

863   Kanai, R., Rees, G., 2011. The structural basis of inter-individual differences in human

864   behaviour and cognition. Nat. Rev. Neurosci. https://doi.org/10.1038/nrn3000

865   Kuntzelman, K., Miskovic, V., 2017. Reliability of graph metrics derived from resting-state

866   human EEG. Psychophysiology 54, 51–61. https://doi.org/10.1111/psyp.12600

867   Lamprecht, R., LeDoux, J., 2004. Structural plasticity and memory. Nat. Rev. Neurosci.

868   https://doi.org/10.1038/nrn1301

869   Laumann, T.O., Gordon, E.M., Adeyemo, B., Snyder, A.Z., Joo, S.J., Chen, M.Y., Gilmore,

870   A.W., McDermott, K.B., Nelson, S.M., Dosenbach, N.U.F., Schlaggar, B.L., Mumford,

871   J.A., Poldrack, R.A., Petersen, S.E., 2015. Functional System and Areal Organization of a

872   Highly Sampled Individual Human Brain. Neuron.

873   https://doi.org/10.1016/j.neuron.2015.06.037

874   Laumann, T.O., Snyder, A.Z., Mitra, A., Gordon, E.M., Gratton, C., Adeyemo, B., Gilmore,

875   A.W., Nelson, S.M., Berg, J.J., Greene, D.J., McCarthy, J.E., Tagliazucchi, E., Laufs, H.,

876   Schlaggar, B.L., Dosenbach, N.U.F., Petersen, S.E., 2016. On the Stability of BOLD fMRI

877   Correlations. Cereb. Cortex 1–14. https://doi.org/10.1093/cercor/bhw265

878   Loh, S., Lamond, N., Dorrian, J., Roach, G., Dawson, D., 2004. The validity of psychomotor

879   vigilance tasks of less than 10-minute duration. Behav. Res. Methods, Instruments, Comput.

880   https://doi.org/10.3758/BF03195580

881   Lohmann, G., Margulies, D.S., Horstmann, A., Pleger, B., Lepsien, J., Goldhahn, D., Schloegl,

882   H., Stumvoll, M., Villringer, A., Turner, R., 2010. Eigenvector centrality mapping for

883   analyzing connectivity patterns in fMRI data of the human brain. PLoS One.

884   https://doi.org/10.1371/journal.pone.0010232

885   Luck, S.J., Vogel, E.K., 1997. The capacity of visual working memory for features and

886   conjunctions. Nature. https://doi.org/10.1038/36846

887   Lydon-Staley, D.M., Ciric, R., Satterthwaite, T.D., Bassett, D.S., 2018. Evaluation of confound

888   regression strategies for the mitigation of micromovement artifact in studies of dynamic

889   resting-state functional connectivity and multilayer network modularity. Netw. Neurosci.

890   https://doi.org/10.1162/netn_a_00071

891   Makris, N., Goldstein, J.M., Kennedy, D., Hodge, S.M., Caviness, V.S., Faraone, S. V., Tsuang,

892   M.T., Seidman, L.J., 2006. Decreased volume of left and total anterior insular lobule in

893   schizophrenia. Schizophr. Res. https://doi.org/10.1016/j.schres.2005.11.020

894   Malykhin, N., Concha, L., Seres, P., Beaulieu, C., Coupland, N.J., 2008. Diffusion tensor

895   imaging tractography and reliability analysis for limbic and paralimbic white matter tracts.

896   Psychiatry Res. - Neuroimaging. https://doi.org/10.1016/j.pscychresns.2007.11.007

897   Mangin, J.F., Rivière, D., Cachia, A., Duchesnay, E., Cointepas, Y., Papadopoulos-Orfanos, D.,

898   Scifo, P., Ochiai, T., Brunelle, F., Régis, J., 2004. A framework to study the cortical folding

899   patterns, in: NeuroImage. https://doi.org/10.1016/j.neuroimage.2004.07.019

900   Mattarella-Micke, A., Mateo, J., Kozak, M.N., Foster, K., Beilock, S.L., 2011. Choke or Thrive?

901   The Relation Between Salivary Cortisol and Math Performance Depends on Individual

902   Differences in Working Memory and Math-Anxiety. Emotion.

903   https://doi.org/10.1037/a0023224

904   McEvoy, L.., Smith, M.., Gevins, A., 2000. Test-retest reliability of cognitive EEG. Clin.

905   Neurophysiol. 111.

906   Mognon, A., Jovicich, J., Bruzzone, L., Buiatti, M., 2011. ADJUST: An automatic EEG artifact

907   detector based on the joint use of spatial and temporal features. Psychophysiology.

908   https://doi.org/10.1111/j.1469-8986.2010.01061.x

909   Motter, A.E., Zhou, C., Kurths, J., 2005. Network synchronization, diffusion, and the paradox of

910   heterogeneity. Phys. Rev. E - Stat. Nonlinear, Soft Matter Phys.

911   https://doi.org/10.1103/PhysRevE.71.016116

912   Moturu, S.T., Khayal, I., Aharony, N., Pan, W., Pentland, A., 2011. Using Social Sensing to

913   Understand the Links between Sleep, Mood, and Sociability, in: 2011 IEEE Third

914   International Conference on Privacy, Security, Risk and Trust and 2011 IEEE Third

915   International Conference on Social Computing. pp. 208–214.

916   https://doi.org/10.1109/PASSAT/SocialCom.2011.200

917   Muldoon, S.F., Bridgeford, E.W., Bassett, D.S., Moreno, Y., Zhou, C.S., 2016. Small-World

918   Propensity and Weighted Brain Networks. Sci. Rep. 6, 22057.

919   https://doi.org/10.1038/srep22057

920   Mullen, T., Kothe, C., Chi, Y.M., Ojeda, A., Kerth, T., Makeig, S., Cauwenberghs, G., Jung,

921   T.P., 2013. Real-time modeling and 3D visualization of source dynamics and connectivity

922   using wearable EEG, in: Proceedings of the Annual International Conference of the IEEE

923   Engineering in Medicine and Biology Society, EMBS.

924   https://doi.org/10.1109/EMBC.2013.6609968

925   Mullen, T.R., Kothe, C.A.E., Chi, Y.M., Ojeda, A., Kerth, T., Makeig, S., Jung, T.P.,

926   Cauwenberghs, G., 2015. Real-time neuroimaging and cognitive monitoring using wearable

927   dry EEG. IEEE Trans. Biomed. Eng. https://doi.org/10.1109/TBME.2015.2481482

928   Newman, M.E.J., 2008. The mathematics of networks, in: The New Palgrave Dictionary of

929 Economics. https://doi.org/doi:10.1057/9780230226203.1064

930 Nierhaus, T., Vidaurre, C., Sannelli, C., Mueller, K.-R., Villringer, A., 2019. Immediate brain

931 plasticity after one hour of brain–computer interface (BCI). J. Physiol. n/a.

932 https://doi.org/10.1113/JP278118

933 Noble, S., Scheinost, D., Constable, R.T., 2019. A decade of test-retest reliability of functional

934 connectivity: A systematic review and meta-analysis. Neuroimage 203, 116157.

935 https://doi.org/10.1016/j.neuroimage.2019.116157

936 Noble, S., Spann, M.N., Tokoglu, F., Shen, X., Constable, R.T., Scheinost, D., 2017. Influences

937 on the Test-Retest Reliability of Functional Connectivity MRI and its Relationship with

938 Behavioral Utility. Cereb. Cortex. https://doi.org/10.1093/cercor/bhx230

939 Nunez, P.L., Srinivasan, R., Westdorp, A.F., Wijesinghe, R.S., Tucker, D.M., Silberstein, R.B.,

940 Cadusch, P.J., 1997. EEG coherency I: Statistics, reference electrode, volume conduction,

941 Laplacians, cortical imaging, and interpretation at multiple scales. Electroencephalogr. Clin.

942 Neurophysiol. https://doi.org/10.1016/S0013-4694(97)00066-7

943 O'Connor, D., Potler, N.V., Kovacs, M., Xu, T., Ai, L., Pellman, J., Vanderwal, T., Parra, L.C.,

944 Cohen, S., Ghosh, S., Escalera, J., Grant-Villegas, N., Osman, Y., Bui, A., Cameron

945 Craddock, R., Milham, M.P., 2017. The healthy brain network serial scanning initiative: A

946 resource for evaluating inter-individual differences and their reliabilities across scan

947 conditions and sessions. Gigascience. https://doi.org/10.1093/gigascience/giw011

948 Onnela, J.P., Saramäki, J., Kertész, J., Kaski, K., 2005. Intensity and coherence of motifs in

949 weighted complex networks. Phys. Rev. E - Stat. Nonlinear, Soft Matter Phys.

950 https://doi.org/10.1103/PhysRevE.71.065103

951 Pannunzi, M., Hindriks, R., Bettinardi, R.G., Wenger, E., Lisofsky, N., Martensson, J., Butler,

952 O., Filevich, E., Becker, M., Lochstet, M., Kühn, S., Deco, G., 2017. Resting-state fMRI

953 correlations: From link-wise unreliability to whole brain stability. Neuroimage.

954 https://doi.org/10.1016/j.neuroimage.2017.06.006

955 Park, H.J., Friston, K., 2013. Structural and functional brain networks: From connections to

956 cognition. Science (80-.). https://doi.org/10.1126/science.1238411

957 Perich, M.G., Gallego, J.A., Miller, L.E., 2018. A Neural Population Mechanism for Rapid

958 Learning. Neuron. https://doi.org/10.1016/j.neuron.2018.09.030

959 Poldrack, R.A., Laumann, T.O., Koyejo, O., Gregory, B., Hover, A., Chen, M.Y., Gorgolewski,

960 K.J., Luci, J., Joo, S.J., Boyd, R.L., Hunicke-Smith, S., Simpson, Z.B., Caven, T., Sochat,

961 V., Shine, J.M., Gordon, E., Snyder, A.Z., Adeyemo, B., Petersen, S.E., Glahn, D.C.,

962 Mckay, D.R., Curran, J.E., Göring, H.H.H., Carless, M.A., Blangero, J., Dougherty, R.,

963 Leemans, A., Handwerker, D.A., Frick, L., Marcotte, E.M., Mumford, J.A., 2015. Long-

964 term neural and physiological phenotyping of a single human. Nat. Commun.

965 https://doi.org/10.1038/ncomms9885

966 Powell, M.A., Garcia, J.O., Yeh, F.C., Vettel, J.M., Verstynen, T., 2018. Local connectome

967 phenotypes predict social, health, and cognitive factors. Netw. Neurosci.

968 https://doi.org/10.1162/netn_a_00031

969 Power, J.D., Barnes, K.A., Snyder, A.Z., Schlaggar, B.L., Petersen, S.E., 2012. Spurious but

970 systematic correlations in functional connectivity MRI networks arise from subject motion.

971 Neuroimage. https://doi.org/10.1016/j.neuroimage.2011.10.018

972 Power, J.D., Lynch, C.J., Silver, B.M., Dubin, M.J., Martin, A., Jones, R.M., 2019. Distinctions

973 among real and apparent respiratory motions in human fMRI data. Neuroimage.

974 https://doi.org/10.1016/j.neuroimage.2019.116041

975   Power, J.D., Plitt, M., Gotts, S.J., Kundu, P., Voon, V., Bandettini, P.A., Martin, A., 2018.

976   Ridding fMRI data of motion-related influences: Removal of signals with distinct spatial

977   and physical bases in multiecho data. Proc. Natl. Acad. Sci.

978   https://doi.org/10.1073/pnas.1720985115

979   Raichle, M.E., MacLeod, A.M., Snyder, A.Z., Powers, W.J., Gusnard, D.A., Shulman, G.L.,

980   2001. A default mode of brain function. Proc. Natl. Acad. Sci. U. S. A.

981   https://doi.org/10.1073/pnas.98.2.676

982   Rubinov, M., Sporns, O., 2010. Complex network measures of brain connectivity: Uses and

983   interpretations. Neuroimage 52, 1059–1069.

984   https://doi.org/10.1016/j.neuroimage.2009.10.003

985   Rypma, B., D'Esposito, M., 1999. The roles of prefrontal brain regions in components of

986   working memory: effects of memory load and individual differences. Proc. Natl. Acad. Sci.

987   U. S. A.

988   Schaefer, A., Kong, R., Gordon, E.M., Laumann, T.O., Zuo, X.-N., Holmes, A.J., Eickhoff, S.B.,

989   Yeo, B.T.T., 2018. Local-Global Parcellation of the Human Cerebral Cortex from Intrinsic

990   Functional Connectivity MRI. Cereb. Cortex. https://doi.org/10.1093/cercor/bhx179

991   Seitzman, B.A., Gratton, C., Laumann, T.O., Gordon, E.M., Adeyemo, B., Dworetsky, A.,

992   Kraus, B.T., Gilmore, A.W., Berg, J.J., Ortega, M., Nguyen, A., Greene, D.J., McDermott,

993   K.B., Nelson, S.M., Lessov-Schlaggar, C.N., Schlaggar, B.L., Dosenbach, N.U.F., Petersen,

994   S.E., 2019. Trait-like variants in human functional brain networks. Proc. Natl. Acad. Sci. U.

995   S. A. https://doi.org/10.1073/pnas.1902932116

996   Shah, L.M., Cramer, J.A., Ferguson, M.A., Birn, R.M., Anderson, J.S., 2016. Reliability and

997   reproducibility of individual differences in functional connectivity acquired during task and

51

998   resting state. Brain Behav. https://doi.org/10.1002/brb3.456

999   Shehzad, Z., Kelly, A.M.C., Reiss, P.T., Gee, D.G., Gotimer, K., Uddin, L.Q., Lee, S.H.,

1000   Margulies, D.S., Roy, A.K., Biswal, B.B., Petkova, E., Castellanos, F.X., Milham, M.P.,

1001   2009. The resting brain: Unconstrained yet reliable. Cereb. Cortex.

1002   https://doi.org/10.1093/cercor/bhn256

1003   Shou, H., Eloyan, A., Lee, S., Zipunnikov, V., Crainiceanu, A.N., Nebel, M.B., Caffo, B.,

1004   Lindquist, M.A., Crainiceanu, C.M., 2013. Quantifying the reliability of image replication

1005   studies: The image intraclass correlation coefficient (I2C2). Cogn. Affect. Behav. Neurosci.

1006   https://doi.org/10.3758/s13415-013-0196-0

1007   Sipos, M.L., Bar-Haim, Y., Abend, R., Adler, A.B., Bliese, P.D., 2014. Postdeployment threat-

1008   related attention bias interacts with combat exposure to account for PTSD and anxiety

1009   symptoms in soldiers. Depress. Anxiety. https://doi.org/10.1002/da.22157

1010   Sorg, C., Riedl, V., Mühlau, M., Calhoun, V.D., Eichele, T., Läer, L., Drzezga, A., Förstl, H.,

1011   Kurz, A., Zimmer, C., Wohlschläger, A.M., 2007. Selective changes of resting-state

1012   networks in individuals at risk for Alzheimer's disease. Proc. Natl. Acad. Sci. 104,

1013   18760 LP – 18765. https://doi.org/10.1073/pnas.0708803104

1014   Thurman, S.M., Wasylyshyn, N., Roy, H., Lieberman, G., Garcia, J.O., Asturias, A., Okafor,

1015   G.N., Elliott, J.C., Giesbrecht, B., Grafton, S.T., Mednick, S.C., Vettel, J.M., 2018.

1016   Individual differences in compliance and agreement for sleep logs and wrist actigraphy: A

1017   longitudinal study of naturalistic sleep in healthy adults. PLoS One.

1018   https://doi.org/10.1371/journal.pone.0191883

1019   Tian, L., Ren, J., Zang, Y., 2012. Regional homogeneity of resting state fMRI signals predicts

1020   Stop signal task performance. Neuroimage 60, 539–544.

1021   https://doi.org/https://doi.org/10.1016/j.neuroimage.2011.11.098

1022 Tuch, D.S., Salat, D.H., Wisco, J.J., Zaleta, A.K., Hevelone, N.D., Rosas, H.D., 2005. Choice

1023   reaction time performance correlates with diffusion anisotropy in white matter pathways

1024   supporting visuospatial attention. Proc. Natl. Acad. Sci. U. S. A.

1025   https://doi.org/10.1073/pnas.0407259102

1026 Van Gaal, S., Scholte, H.S., Lamme, V.A.F., Fahrenfort, J.J., Ridderinkhof, K.R., 2011. Pre-

1027   SMA graymatter density predicts individual differences in action selection in the face of

1028   conscious and unconscious response conflict. J. Cogn. Neurosci.

1029   https://doi.org/10.1162/jocn.2010.21444

1030 Vinck, M., Oostenveld, R., Van Wingerden, M., Battaglia, F., Pennartz, C.M.A., 2011. An

1031   improved index of phase-synchronization for electrophysiological data in the presence of

1032   volume-conduction, noise and sample-size bias. Neuroimage 55, 1548–1565.

1033   https://doi.org/10.1016/j.neuroimage.2011.01.055

1034 Wei, X., Yoo, S.S., Dickey, C.C., Zou, K.H., Guttmann, C.R.G., Panych, L.P., 2004. Functional

1035   MRI of auditory verbal working memory: Long-term reproducibility analysis. Neuroimage.

1036   https://doi.org/10.1016/j.neuroimage.2003.10.039

1037 Westerhausen, R., Kreuder, F., Woerner, W., Huster, R.J., Smit, C.M., Schweiger, E., Wittling,

1038   W., 2006. Interhemispheric transfer time and structural properties of the corpus callosum.

1039   Neurosci. Lett. https://doi.org/10.1016/j.neulet.2006.09.028

1040 Yantis, S., Schwarzbach, J., Serences, J.T., Carlson, R.L., Steinmetz, M.A., Pekar, J.J., Courtney,

1041   S.M., 2002. Transient neural activity in human parietal cortex during spatial attention shifts.

1042   Nat. Neurosci. https://doi.org/10.1038/nn921

1043 Yeh, F.C., Vettel, J.M., Singh, A., Poczos, B., Grafton, S.T., Erickson, K.I., Tseng, W.Y.I.,

1044   Verstynen, T.D., 2016. Quantifying Differences and Similarities in Whole-Brain White

1045   Matter Architecture Using Local Connectome Fingerprints. PLoS Comput. Biol.

1046   https://doi.org/10.1371/journal.pcbi.1005203

1047

1048

1049